THESIS FOR THE DEGREE OF LICENTIATE OF ENGINEERING

Characterization of artificial and biological lipid vesicles using TIRF and SPR

THOMAS OLSSON

CHALMERS

Department of Applied Physics

CHALMERS UNIVERSITY OF TECHNOLOGY

Gothenburg, Sweden 2018

Characterization of artificial and biological lipid vesicles using TIRF and SPR

THOMAS OLSSON

Department of Applied Physics
Chalmers University of Technology
SE-412 96 Gothenburg
Sweden
Telephone + 46 (0)31-772 1000

Printed at Chalmers Reproservice
Gothenburg, Sweden 2018

Characterization of artificial and biological lipid vesicles using TIRF and SPR

THOMAS OLSSON

Department of Applied Physics, Chalmers University of Technology

Abstract

Synthetic lipid vesicles serve as important mimics of cells and the natural membranes that they are enclosed by. As such they are frequently used as simplified models of the highly complex cell membrane to aid in-depth physicochemical and biological characterization of this essential biological structure. Lipid vesicles also fulfill fundamental biological functions, for example in intercellular signaling via extracellular vesicles and also as signal-substance containing intercellular secretory vesicles in the synapses of neurons and in secretory cells of the endocrine glands, which release their cargo to the extracellular space in response to external cues. Lipid-based nanoparticles are also of increasing importance as drug carriers, both for targeted release at specific tissues and for improved cellular uptake.

There are today many techniques available to probe a multitude of lipid vesicle properties, including size, structure, content, molecular composition etc. In this thesis work, we have contributed improved means to quantify vesicle size using fluorescence microscopy by using total internal reflection fluorescence (TIRF) microscopy to correlate the measured distribution in fluorescence intensity of individual vesicles to their size, as measured by nanoparticle particle tracking analysis (NTA). A similar approach has been used before by others, but the formalism used that have won prevalence contains a mathematical error, which motivated the introduction of an improved expression for converting total vesicle intensity to vesicle size. We present the difference between the former and the latter formalism, as well as the possible negative impact of the former when used to draw conclusions for larger sized vesicles in a number of studies. One example when this type of analysis is crucial, is in studies were a certain vesicle property is correlated with vesicle size. One such example is studies of membrane protein function, which is often dependent of membrane curvature.

In the second work, we used surface plasmon resonance (SPR) and amperometry as quantitative methods to investigate whether secretory dense core vesicles, isolated from bovine chromaffin cells from the medulla of adrenal glands, are able to maintain their high loading of catecholamine molecules after vesicle isolation and purification and how the vesicle catecholamine content is affected by vesicle exposure to osmotic stress. We found, as also previously reported by intracellular amperometry measurements in live cells, that dense core vesicles release part of the vesicle catecholamine content when exerted to a hyperosmotic shock, and also that this release occurs very rapidly in response to the applied osmotic stress. This work demonstrates the strength of using different complementary label-free measurements to account for the total number of catecholamine molecules in such vesicles and for monitoring molecule release from vesicle compartments in real-time. Further, by using knowledge gained about chromaffin vesicle size from TEM together with changes in refractive index as probed with SPR using suspensions based on ordinary and heavy water, we could estimate the hydration level of the dense protein core of the chromaffin vesicles.

Keywords. membrane permeability, liposome, vesicle, large dense core vesicles (LDCVs), cell membrane, fluorescence, total internal reflection (TIRF) microscopy, nanoparticle tracking analysis (NTA), surface plasmon resonance (SPR), osmotic shock, chromaffin vesicle

List of appended papers

The thesis is based on the work contained in the following articles.

I. Total internal reflection fluorescence microscopy for determination of size of individual immobilized vesicles: Theory and experiment
T. Olsson, V. P. Zhdanov, and F. Höök,
J. Appl. Phys., vol. 118, no. 6, p. 064702, Aug. 2015.

II. Content and Dense-Core Quantification of Chromaffin Vesicles using Surface Plasmon Resonance
Fathali, H. M.,[1] Olsson, T.,[2*] Hook, F.[2] and Cans, A-S.[1,**]*
Manuscript in preparation

Contribution to the appended papers

I. I planned, performed and analyzed the experiments. I wrote parts of the manuscript.

II. I planned, performed and analyzed the experiments with Hoda. I wrote the main part of the manuscript together with Hoda.

Publications not included in the thesis

III. Hydrodynamic separation of proteins in supported lipid bilayers confined by gold barriers
Björn Johansson, Thomas Olsson, Peter Jönsson and Fredrik Höök
Soft Matter 9, 9414-9419 (2013).

I planned and performed the experiments, analysis together with Björn. I wrote parts of the manuscript.

List of abbreviations

TIRFM	Total Internal Reflection Fluorescence Microscopy
POPC	1-palmitoyl-2-oleoyl-sn-glycero-3-phosphatidylcholine
DMPC	1,2-dimyristoyl-sn-glycero-3-phosphocholine
SPR	Surface Plasmon Resonance
NTA	Nanosight Tracking Analysis
Cy5	Cyanine fluorophore
SUV	Small Unilamellar Vesicle
LUV	Large Unilamellar Vesicle
GUV	Giant Unilamellar Vesicle
MLV	MultiLamellar Vesicle
SLB	Supported Lipid Bilayer
SDS	Sodium Dodecyl Sulfate
FRAP	Fluorescence Recovery After Photobleach
FRET	Fluorescence Resonance Energy Transfer
TEM	Transmission electron microscopy
AFM	Atomic Force Microscopy
QCM-D	Quartz Crystal Microbalance with Dissipation
NA	NeutrAvidin
SA	Streptavidin
PLL	Poly-L-lysine
PLL-g-PEG	Poly-L-lysine-grafted Polyethylene Glycol
PEG	Polyethylene Glycol
HS-PEG	Thiol-Polyethylene Glycol
ATP	Adenosine triphosphate
ADP	Adenosine diphosphate
NMR	Nuclear magnetic resonance

Table of Contents

1 Introduction

Background

Cells are the fabric of life, at least from a biological point of view. One cell is the definition of the smallest living entity, while 10^{13} collaborating cells with a specific blueprint in their DNA makes up a fully grown human. Thus, to understand cells and their components is at the very base of understanding biological life, also in the form of multicellular organisms like us. Functionality and dysfunctionality and disease could all eventually be traced down to the cellular level. It is thus not surprising that about 70% of all pharmaceutical drugs target proteins situated in the membranes enclosing the cells.[1]
However, cells are highly crowded and complex in their function and composition, which is also true for their enclosing membranes (see section 2.1 and 2.2). Thus, many times, the cellular environment offers a far too complex environment for most types of physical and chemical characterizations. Now, the underlying structure of the cell membrane is made up of a lipid bilayer (fig.5), and ever since the 60's, artificial spherical shells made up by a single lipid bilayer have been used as a simplified construct or model closely resembling one basic structure of the cell membrane (fig.11).[2] These lipid vesicles have since been used as a model system to explore and characterize a multitude of cellular functions and components such as proteins, enzymes, membrane fusion, effect of lipid composition on properties such as membrane rigidity, permeability and much more.[3–5] Detailed investigations of this type are often dependent on an initial characterization of the sizes of the vesicles used, which may indeed affect the conclusions drawn from any subsequent characterizations made. For example, it is required to know the vesicle size to be able to compare release kinetics for different vesicle samples and values in literature.

Surface sensitive techniques

Cells and cellular components are in the size range of >0.1 nm to ~10 μm, with proteins typically in the range of a few nm in size. However, for most biological material, the limit of what can be visualized with conventional light microscopy is typically around 200 nm for biological samples. For that reason there has been a strong development over the last ~50 years to construct instruments sensitive enough and with high enough resolution to be able to study and characterize cellular components smaller than that, including how they interact with each other. Some of the most sensitive techniques are surface based. One important such instrument is surface sensitive fluorescence microscopy, where fluorescent molecules called fluorophores are conjugated to the molecules intended for study, can make it possible to visualize down to single molecules. Another technique is surface plasmon resonance, which is an instrument with very high sensitivity, capable of detecting small changes in refractive index close to the sensor surface. With increase in sensitivity and resolution of sensing techniques it is possible to get a more detailed understanding of cells and their components, which is important to further the development in medicine, and carries as a result the opportunity of identifying new drug targets and the possibility to develop new treatments. In particular, a prerequisite for improving the understanding of the cell membrane, is a possibility to characterize properties such as size, permeability and affinities between different biomolecules.

Thesis statement

In the first work included in this thesis, we contribute to an improvement of in situ size characterization of individual vesicles based on their fluorescence intensity, when probed by TIRF microscopy. In early studies, reconstitution of proteins and membrane bound enzymes into lipid vesicles have been employed without carefully considering the size (curvature) of the lipid vesicles used. However, it has later been shown that vesicle size does affect properties like enzymatic activity, lipid-protein interaction (protein function) and membrane fusion.
When vesicles are artificially made, the resulting vesicles always come in a distribution of sizes. The distribution may be narrow or wide, depending on a number of aspects, such as the size aimed for and the protocol used for preparation. Typically, smaller vesicles have more narrow size distribution, while larger ones may have considerably large distributions. Many times ensemble measurements techniques are used, which provide an average signal of whatever property that is studied for the whole vesicle size distribution, thereby concealing any heterogeneity that may relate to vesicle size. To probe the influence of membrane curvature, three different size distributions of vesicles have been used; however, it was found that these size distributions could overlap as much as about 70%[6]. To improve this, Stamou's group developed a technique to determine size of individual vesicles from the recorded fluorescence intensities obtained using TIRF microscopy[6,7]. This technique made it possible to study several hundred vesicles of different sizes in the same measurement. In this way, for example, the dependence of membrane protein function on the membrane curvature was more readily observed. However, it was also found that while the model for converting total intensity of a lipid vesicle to vesicle size worked well for smaller sized vesicles, a mathematical error meant that the sizes of larger vesicles were grossly overestimated. We found that an erratic model had been used in this and several subsequent papers to offer claims for the effect of larger sized vesicles on for example protein function. Our contribution in this field, was to offer a corrected model along with a strategy to more accurately convert fluorescent intensity to size even for the larger sized vesicles (**paper I**).

In the second work we use a label-free technique (surface plasmon resonance (SPR)) to characterize chromaffin lipid vesicles isolated from adrenal glands, which are used in the body for storing and storing the signaling substances adrenaline and nor-adrenaline at high concentrations. These chromaffin vesicles enclose a dense protein core which binds most of the adrenaline and nor-adrenaline. By employing SPR, we developed in **paper II** a new method to probe the molecular volume of the dense core.
Secretory chromaffin vesicles, have previously been studied with various techniques,[8] more lately by different versions of amperometry.[9] We employed a new purification protocol for the biological samples, which also serves to narrow down the size distribution of the studied vesicles, capable as it seems to maintain the initial catechol loading of the vesicles. In the next step we immobilized the purified chromaffin vesicles on a chip in a surface sensitive technique, surface plasmon resonance (SPR), where we were able to observe partial release of the initial catechol loading by hyperosmotic challenges. We also employed a switch with buffer based on H_2O or D_2O, to study changes in net refractive index. By this approach, we could quantify the volume occupied by the dense protein core inside of the chromaffin vesicles. Further, by comparison to transmission electron microscopy (TEM) images, with negatively stained protein core,[10] we could estimate the hydration level of the dense protein core (**paper II**). By observing induced release and by using values of the refractive index of catecholamines together with resolving the dimensions of the chromaffin vesicles, we were able to estimate the number of released catecholamines per vesicles and what vesicular concentration this would correspond to.

Outline

The thesis starts with a short introduction to the cell, its complexity and its constituent parts, including a section about the cell enclosing membrane and its functions and key properties. After this are presented a number of different simplified models designed to study cell membranes and membrane incorporated components. We look closer at lipids, lipid vesicles and properties of the lipid membrane. Then comes an overview of vesicles used in combination with surface sensitive techniques, after which follows a look at the different techniques used in this thesis. Finally, there is a summary of the results, conclusion and outlook.

2 The living cell

Cells were first discovered by Hooke in 1665, as he made observations of cellular structures when looking at thin slices of cork in a microscope (**fig. 1**) [11]. He went on to observe that these structures were commonly present in other plant species that he studied.

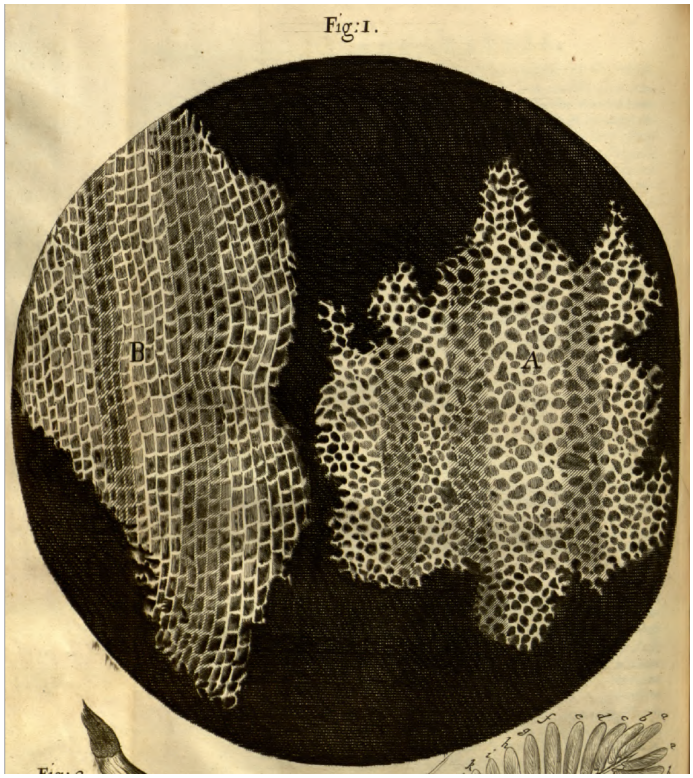

Fig. 1. *Hooke's illustration details cells from thin slices of cork cut along the direction of the fibers to the left and from a slice perpendicular to the right.*

Cells are essential building block that are required for all forms of biological life on our planet (**fig. 1**). The cells carry, within their nucleolus, all the information of their particular species. This information and life itself is passed down through the generations of the organism to which it belongs. In multicellular organisms as plants and animals, all cells communicate, cooperate and put the common good above the individual. All multicellular organisms starts off with one cell, which then goes on dividing itself by mitosis (making clones of itself), so all cells in any multicellular organism have the first cell as their ancestor. Seen in this light, the extreme level of communication, cooperation between cells required for the organism to function and the unquestioned self-sacrifice of individual cells for the common good is perhaps more understandable. That first cell does not only duplicate, but the new cell copies also diversifies into about 200 different cell types[12], these new cells also migrates to particular locations, everything as orchestrated by the blueprint in the DNA (~10^{13} cells in the human body[13]). One can marvel at the incredible level of communication and cooperation needed of the ever increasing number of cells during the development to eventually form a complete organism. To ensure proper function, the completed organism then needs to maintain a very high level of communication and cooperation between the cells, that scales with the complexity of the organism, throughout its entire life-span. Cells within organisms are also replaced over time at relatively high rates (~10^{8} per day in the human body). It perhaps does not come as a surprise then that all functions or dysfunctions and diseases of the human body could eventually be traced down to the cellular level. For instance, about 70% of all medications target different proteins located in the enclosing membrane of the cell. A lot more could be stated, but this

suffice as a starting point for realizing the importance of learning all we can about the cell and its functions.

2.1 Composition of the eukaryotic cell

The eukaryotic cell is enclosed by a plasma membrane which works both as a shell, protecting the cell from the outside environment, and as a boundary, regulating molecular transport across the membrane as well as providing means of communication with other cells. The cell contains about 20 different types of organelles, situated in the cytoplasm (inside solution). The organelles could be called the machinery of the cell, each providing different services to the cell. For example, the *mitochondria* is involved in turning nutrients into energy (ATP), needed to drive various reactions in the cell. The *endoplasmic reticulum* (ER) synthesizes lipids and proteins and acts as storage for Ca^{2+} ions. Once the lipids and proteins are synthesized, the ER passes them on to the *Golgi apparatus* where they may be further modified before they are passed on to the intended recipients. The *lysosome* is the cellular destruction center where everything marked for destruction is brought and degraded.

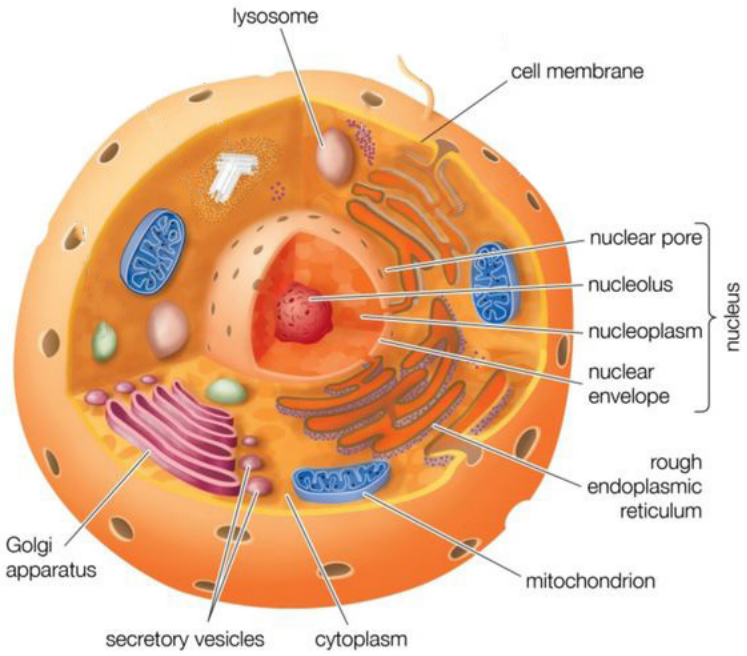

Fig. 2. *Illustration of an eukaryotic animal cell and its organelles.*

Central to all cell types within our bodies is the nucleolus which contain the blueprints of the organism in its DNA, with exception for the red blood cells in which it is ejected in favor of the oxygen carrying protein hemoglobin. It is the nucleolus that directs the cell function with intracellular and extracellular communication through chemical signals and RNA, which regulates expression (production) of all different proteins and enzymes needed for survival. *Secretory vesicles* buds off from the *Golgi apparatus,* and are cargo vesicles capable of storing high concentrations of molecules intended for extracellular release via exocytosis. These can for example be the large dense core vesicles (LCDVs) that we study in **paper II**.

2.2 An important Organelle for cell communication- The secretory vesicle

Secretory vesicles are present in all cells (**fig.2**), but the ones found in nerve cells and chromaffin cells plays key roles in central bodily communication systems (nervous and endocrine system) by providing rapid chemical communication in response to specific stimuli. The different secretory vesicles span a wide range of sizes; the synaptic vesicles found in the synapses of the nerve cells are the smallest ones ~4-60 nm (**fig. 3A-C**), they relay nerve signals to the next nerve cells in the chain or to intended muscle cells by releasing their signaling substance cargo into the synaptic cleft, which diffuse and dock to a receptor at the recipient and the signal is relayed. The large dense core vesicles (LCDVs) found in chromaffin cells in the adrenal glands are ~150-900 nm, they contain high concentrations of signaling substances (dopamine, adrenaline, noradrenaline), the dense protein core enables storage of high concentrations, to be released for long range communication in the body (**fig16**). The largest secretory vesicles ~1-10 μm are found in the gut providing mucus to the lining of the intestines[1415]. The secretory vesicles have in common that they are enclosed by vesicular membranes with very specific lipid and protein compositions. In these membranes, there are proteins for transport in and out of the vesicles of the cargo, as well as targeting proteins for docking to the cell membrane (**fig.3C**) and special SNARE proteins for fusing[16,17] during exocytosis (the process where the vesicles migrate to the cell membrane and fuse for release of cargo to the outside of the cell).

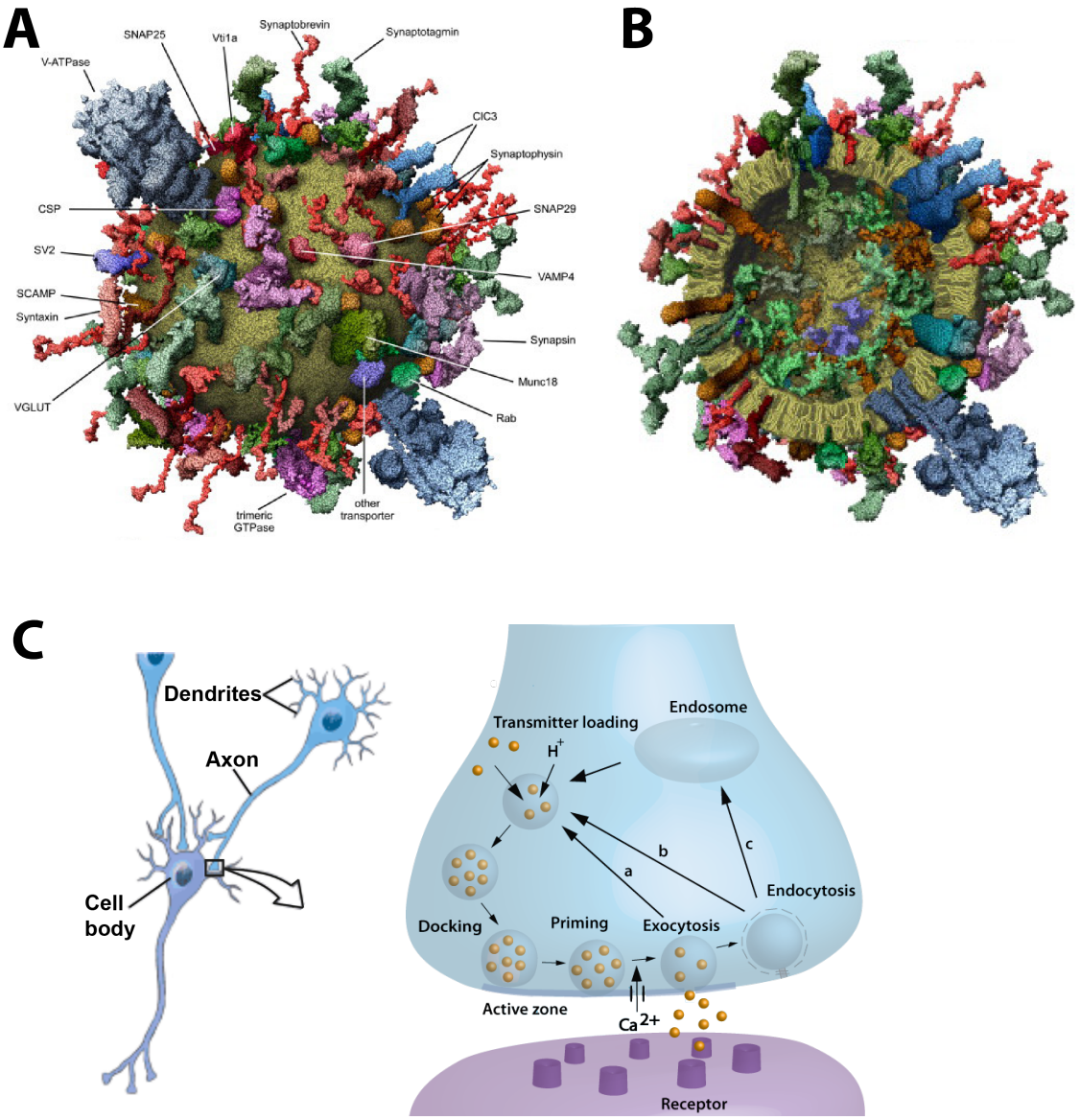

***Fig. 3.*(*a*)** *An illustration of a synaptic vesicle with detailed composition. (**b**) A cut-through of the vesicle. Image from* [12]*. (**c**) Left, connected nerve cells. Right showing an enlargement of one of the contact points between two nerve cells with illustrations of synaptic vesicles during loading of transmitter substances, exocytosis (fusing with the membrane to release transmitter substances to the synaptic cleft) and endocytosis (vesicles budding off from the membrane after transmitter release to be recycled). Unenlarged part of image (c) from* [18]*.*

The synaptic vesicles in nerve cells store transmitter substances at high concentrations (**fig.3C**). Upon receiving specific signals, these vesicles migrate rapidly out to the plasma membrane and release the transmitter substance, into the synaptic cleft, as a means of relaying the nerve signal to another nerve or muscle cell. In **paper II** we look closer at secretory vesicles used in the endocrine signaling system, called chromaffin vesicles (**fig.4**). These vesicles are found in chromaffin cells located in the adrenal glands, and subpopulations store high concentrations of either adrenalin, nor-adrenalin or glutamate, bound to a dense core protein matrix and also in aggregates with ATP in the intravesicular space (unbound catecholamines can pass through the lipid membrane). Upon a specific signal one of these subpopulations of vesicles rapidly migrate

out to the plasma membrane and release their transmitter substance which is then carried to all parts of the body via the bloodstream.

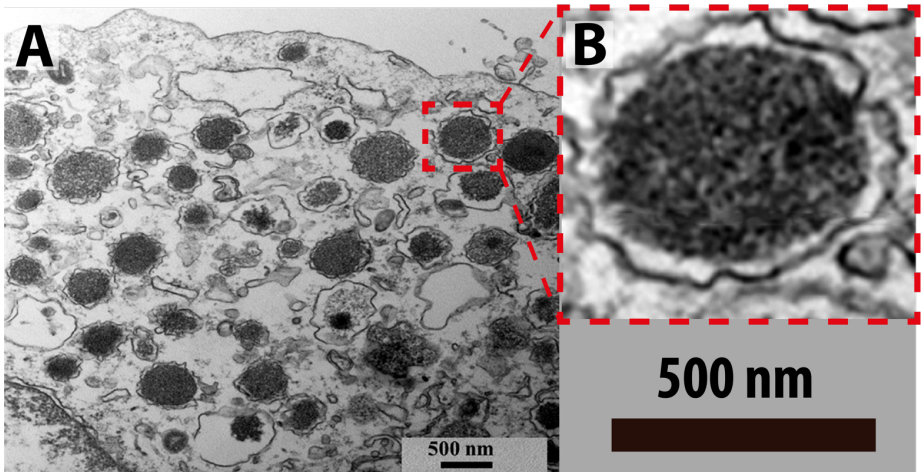

Fig. 4. *(**a**) TEM images of large dense core vesicles (LDCVs) inside a chromaffin cell (the protein dense cores have been dark stained). (**b**) Close-up of one of the LDCVs. Image modified from* [19].

The process of delivering substances out of the cell with the help of vesicles, in such a way that the substances does not have to physically cross the plasma membrane, is called exocytosis (**fig.15a**). The reverse process, by which the cell brings in substances by vesiculation or intake of intact vesicles from the outside is called endocytosis (**fig.15b**). Apart from the direct release of substances to the outside of the cell, there are also cargo vesicles which are secreted intact from the cells without first fusing with the plasma membrane. These vesicles, called exosomes, carry targeted communication cargo (for long-range targeted communication), sometimes in the form of RNA (**fig.5** [20,21]. The specificity of the targeting by the exosomes comes from their enclosing membranes being highly functionalized with targeting molecules used for docking at the intended recipient.

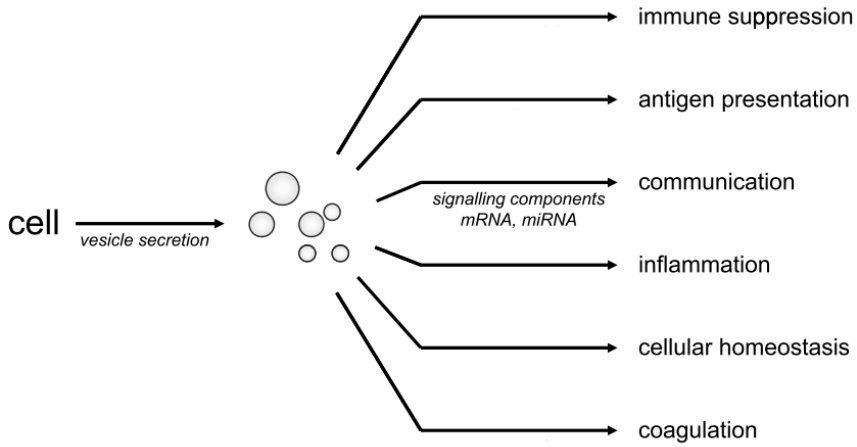

Fig. 5. *Showing some different types of intact vesicle secretions from cells. Image adapted from* [20]

It is in the context of the function of secretory vesicles relevant to recall that in nerve cells, the secretory vesicles carry out short-range communication, while the secretory chromaffin vesicles carry out long-range intercellular communication. A majority of these two types of secretory vesicles are recycled within the cells, as they mostly seem to fuse locally at the plasma membrane, releasing their transmitter substances through a pore before detaching again [22]. In **paper II**, we investigated isolated chromaffin vesicles.

3 The cell membrane

The cell and all its sub compartments (organelles) are enclosed by highly functionalized membranes. The membrane enclosing the cell is called plasma membrane. Perhaps the foremost role of these membranes is to separate inside from outside, i.e. provide a different operational environment on the inside compared to the surrounding chemical balances outside. The composition of the plasma membrane and each membrane surrounding different organelles are quite different in their lipid composition and also in amount and types of incorporated proteins, in principle this is to provide the right membrane function for what the particular membrane encloses.

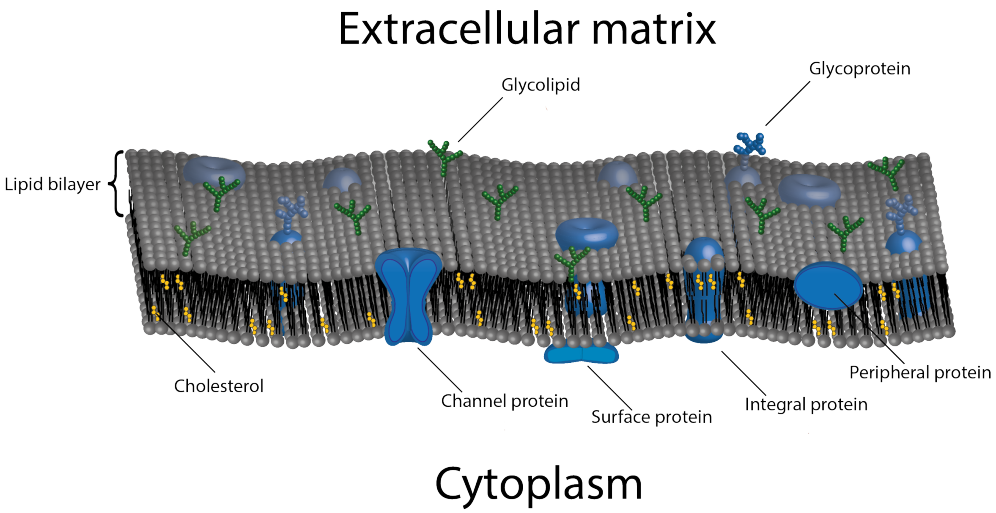

Fig.6 *Simplified illustration of a cell membrane. The backbone of the membrane consists of a bilayer of lipids, within and attached to this backbone are functionalised proteins and sugar modified lipids and proteins. All carbohydrates (sugars) are located towards the extracellular matrix (outside of the cell).*

While highly functionalized with proteins and sugars, the "backbone" of the cell membrane is made up of a lipid bilayer (**fig.6**). The composition of the cell membrane is highly complex, and contains for example made up of up to 1000 different types of lipids. Of the lipids, about 5% of those located in the outer leaflet are functionalized with sugar molecules. There is also a high heterogeneity in the lipid compositions of the inner and outer leaflet of the cell membrane, meaning the inner and outer leaflet mostly contain different types of lipids. Further, there is a large amount of different incorporated membrane proteins, making up about 50% of the cell membrane mass,[23] providing a range of added functionality. The fluid mosaic model of the cell membrane,[24] describes each leaflet of the cell membrane as a two-dimensional fluid with free lateral movement for the lipids and proteins. In addition, cell membranes are flexible and could be deformed by bending, stretching, shearing and lateral compression [25,26] (**fig.14**). Many important cell functions are based on a combination of the flexibility and lateral fluidity of the membrane, as cell migration, exocytosis, endocytosis and intercellular communication via nanotubes and exosomes. Importantly, even without the functionalization of the membrane components with sugars and proteins, the lipid bilayer with its hydrophobic core provides basic functionality to the cell by its highly selective permeability to different molecules. One of the key features of the cell membrane is its ability to retain osmotic imbalance (unequal concentrations of, for example, ions inside the cell compared to outside). An example of this barrier function is found in **paper II**, where the LDCVs are able to maintain pH 5.5 inside while the outside pH is 7.4. Initially, this is achieved by a membrane incorporated proton pump H^+-ATPase which with energy from ATP shuttles protons H^+ from the outside to the inside[27]. However, once this imbalance is

achieved, the membrane in itself serves as a barrier able to maintain the H^+ imbalance for a long time (for permeability of ions across membranes, see **fig.7**)

3.1 Cell membrane permeability

The cell membrane acts as a restricting barrier for chemical transport in and out of the cell. The lipid bilayer which makes up the backbone of the cell membrane is semipermeable to different solutes. While highly permeable to water and other small polar solutes it is virtually impermeable to ions and large nonpolar solutes like sucrose (**fig. 7**)[23]. It is quite amazing that even without any functionalizing protein transporters, a lot of the requisites for many of the basal cell functions are provided solely by the selective permeability of the lipid bilayer. The cell membrane is highly permeable to water, but also to glycerol (nutrient) and urea (waste), O_2 and CO_2, which all play a key role in the cells basic functions. The high resistance to ions makes it possible to maintain an ionic imbalance which is used for virtually all energy transfers within the cell (ADP to ATP).

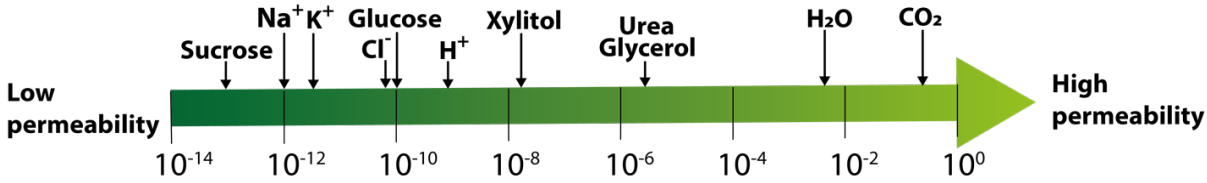

Fig.7 *Showing typical permeabilities (cm/s) of some common solutes across lipid bilayers*[28–31] *in Log-scale. Figure adapted from* [23].

To put some differences in permeability in context. Water is known to equal out osmotic pressure, in a process called osmosis (flow of water across the membrane induced by a gradient in solute concentration), across the membrane of small vesicles through simple diffusion in about 25 ms (**fig.8.2**). Larger permeable molecules like xylitol on the other hand, takes about 8 min to reach iso-osmolar condition in similar sized vesicles (**fig.8.3-4**).
Membrane and lipid bilayers with different compositions will be differently permeable towards the same solute depending on their variation in lipid composition. The feature that seems to affect permeability the most is the average distance between the physical headgroups of the lipids in the membrane (depends on lipid composition, larger distance between physical headgroups, higher permeability).[32] Permeability across the same membrane will also change with temperature (as it affects both diffusion speeds of solutes and of lipids in the membrane).[33] Depending on the temperature the lipids in the membrane could either be in liquid or gel-state (the latter at low temperatures, permeability typically sinks more than an order of magnitude when bilayers are in gel-phase).[34] Membrane permeability is also regulated by the concentration of cholesterol and sphingolipids in the membrane, as addition of these increase the membrane packing density (higher conc. cholesterol/sphingolipids, lower permeability).[32,35,36]

The driving force behind passive transport across the membrane is diffusion. Diffusion is the random Brownian motion of molecules, driven by thermal energy, in liquid or gas phase which makes them spread out until reaching an equilibrium concentration in their whole confinement. Solute molecules or particles in a solvent diffuse in a similar fashion to gases in air, this creates a pressure on the enclosing container. For solute molecules in a solvent (like water) this is called osmotic pressure and is the cause of osmosis and passive transport across lipid membranes.
The diffusivity of a spherical particle could be described by the Stokes-Einstein equation

$$D = \frac{k_B T}{6\pi\eta r} \quad (1)$$

, where k_B is the Boltzmann constant, T temperature in K, η is the viscosity of the solution and r is the particles hydrodynamic radius.[26] This relation is used to determine the size of for example lipid vesicles in NTA and DLS (the diffusivity D is in these cases obtained from single particle tracking analysis). As could be seen in eq.1 (with all other parameters fixed), the diffusivity scales with the hydrodynamic radius of the particle. This means that smaller molecules and particles diffuse faster than larger ones.

Osmolarity could be said to be the concentration of osmotically active molecules per liter, it is usually given in mOsm. A concentration of 100 mM NaCl, would correspond to an osmolarity of 200 mOsm as NaCl ionize fully into Na^+ and Cl^- at moderate concentrations, while a concentration of 300 mM xylitol on the other hand would correspond to an osmolarity of 300 mOsm.

An illustration of osmotic regulation and loading/unloading by passive diffusion could be seen in **fig. 8**, portraying the case of simple diffusion across vesicle membranes when introducing osmotic stress with a permeable solute such as xylitol. During osmotic response upon introduction of some impermeable solute, as sucrose like we used to induce hyperosmotic shock in **paper II**, the vesicles will stay in state **2** (**fig. 8.2**) until the osmotic stress is removed, it will then go back to the original shape. In the figure we notice, as often found for different kinds of vesicles, that during hyperosmotic shock, they do act as perfect osmometers. This was found for red blood cell ghosts[37], chromaffin vesicles[38] and different lipid vesicles.[39] This means that the vesicle by local deformations and ejection of water are able to equilibrate the osmotic pressure on both sides of the vesicle membrane. Vesicles are most commonly reconstituted in a buffer close to physiological conditions, so at state 1 in figure 7, the outside and inside of the vesicles are thought to contain impermeable solutes that provide about 210 mOsm osmotic pressure at equilibrium (100 mOsm Na^+, 100 mOsm Cl^- and 10 mOsm Tris). The presence of impermeable solutes inside the vesicles makes it possible for osmotic equilibrium to be achieved by reducing the vesicle volume until the osmotic pressure inside corresponds to the one on the outside. The volume changes of a perfect osmometer could be said to agree with Boyle-van't Hoff's law reformulated as:

$$V_1 = \frac{c_0}{c_1} V_0 + V_{\text{membrane}} \quad (2)$$

, where V_1 is the new outer vesicle volume after equilibration, c_0 is the osmolarity inside the vesicle at its initial inner volume V_0, c_1.is the induced osmolarity outside and V_{membrane} is the osmotically inactive part of the vesicle volume. Local deformations are more energy efficient than longitudal and lateral compression, which is why the former has been found to happen during low-moderate hyperosmotic shock (depending on lipid composition).[40–43] For hypoosmotic shock, during unloading, we notice that the swelling seen at stage **5**, is not enough to equilibrate the osmotic pressure (**fig. 8.5**). The reason for this is that it requires a much higher energy cost to go from spherical shape to expanded spherical shape as this requires a stretching of the whole membrane[44]. More simply put, we can compare this resistance to stretching of the membrane to the resistance felt when inflating a balloon, a lot of pressure is needed for inflation, meaning air pressure inside will be much higher than outside. In a similar way, for the membrane it is possible to absorb the osmotic pressure energy, and thereby maintain an osmotic imbalance, as the energy gained by the shielding of the hydrophobic membrane parts is greater. This means that for a 300 mOsm hypoosmotic shock (**fig.8.5-6**, as the outside of the loaded vesicles is changed to buffer without solute), the expansion would correspond to about 2-3% increase in volume.[45] If one calculates the volume increase needed to equilibrate the osmotic

pressure with eq.2, we get a required volume increase of ~+140%. Even for very high hypoosmotic gradients (>1 Osm), there are limiting factors to the osmotic response. For vesicles that are spherical to begin with, they can only expand/stretch the membrane area up to between 6-9% depending on size and lipid composition before transient pore formation and lysis (bursting) [45–48], for smaller vesicles at > 1 Osm[4546]. The 6-9% increase in surface area would correspond to a volume increase of about 9-14%. As xylitol empties out (**fig.8.6-7**), the vesicle contracts from this swollen state until it has regained its original volume.
To sum up, during loading (hyperosmotic shock), the vesicle volume changes correspond directly to the osmotic gradients, but the corresponding vesicle volume changes during unloading (hypoosmotic shock) are rather insignificant in comparison (due to high energy cost of membrane stretching).

In TIRF microscopy it is only possible to study solute transport during loading, as transport is studied indirectly as changes in vesicle volume, as it is for osmotic shrinkage and reswelling that vesicles behave as perfect osmometers (**fig.8.1-4**). Most alternative vesicle based techniques used to measure permeability also study permeability indirectly as changes in volume during solute loading, such as changes in light scattering intensity in stopped flow[49], quenching of fluorophores in stopped flow[50–52], light microscopy studies of GUVs[53] and NMR[54,55]. However, in SPR, one has to instead look at unloading, this is because the strong osmotic shrinkage/reswelling during solute loading (**fig.8.1-4**) leads to a strong contribution to the signal, this as lipid membrane material will move closer to the sensor surface during shrinking (**fig.8.2**) and away again during reswelling (**fig.8.3**), lipid membrane movement during loading thereby masks the transport signal. For solute unloading, the vesicle deswelling is very small and only makes up a minor part of the measurement signal (**fig.8.5-7**), the major part stemming from refractive index changes inside the vesicles.

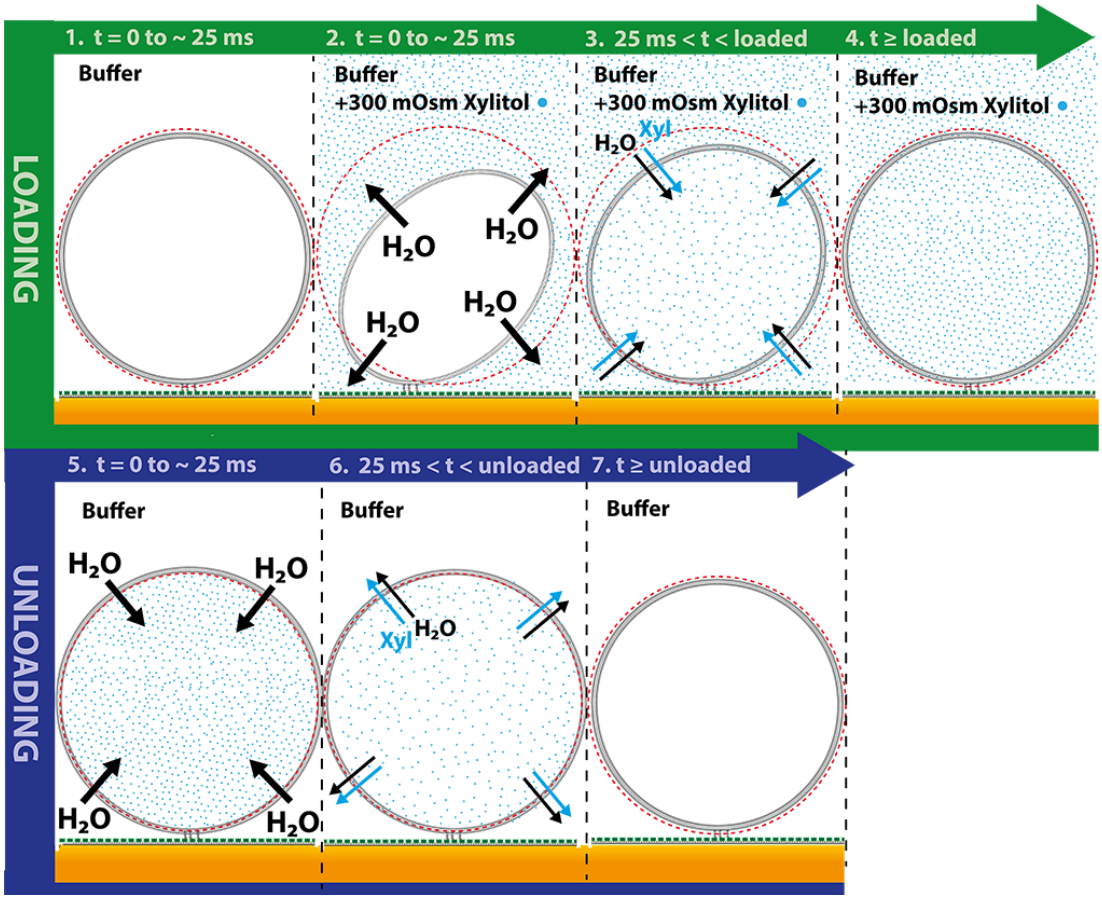

Fig.8 *Illustration of how a single lipid composition SUV changes volume during vesicle loading and unloading. (**1**) Initial volume of vesicle filled with buffer (100 mM NaCl + 10 mM Tris in buffer not shown). (**2**) An introduced osmotic gradient makes water rapidly exit from the vesicles in order to equilibrate inside and outside osmolarity. (**3**) As xylitol starts to fill the vesicle, water comes back to keep osmotic equilibrium. (**4**) When fully loaded with xylitol, the vesicle has regained its initial volume. (**5**) Switching to just buffer outside leads to water quickly rushing into the vesicle and the vesicle area expands perhaps 2-3%. (**6**) As xylitol goes out, so does the water until the vesicle has emptied out all xylitol and regained its original volume in (**7**).*

When measuring solute transport across lipid membranes, the signal response ΔR (for unloading, if only dependent on the transport) could be described with a single exponential as

$$\Delta R = A \cdot e^{-kt} \tag{3}$$

, where A represents the loading amplitude and k is the transport rate of the solute. Now, the transport rate for the same solute will be different for different sized vesicles, which is why permeability is a preferred parameter used to compare different membranes and solutes. Permeability across vesicular membranes is defined as

$$P = \frac{k \cdot V_{\text{ves}}}{A_{\text{ves}}} = \frac{k \cdot r_{\text{ves}}}{3} \tag{4}$$

, where k is the measured transport rate across the membrane, V_{ves} is the vesicle volume, A_{ves} is the membrane area and r_{ves} is the radius of the vesicle.

By combining permeability with Fick's first law, the flux of molecules across a membrane *J* in ($mol \cdot cm^{-2} \cdot s^{-1}$) could be described as

$$J = P\Delta C \quad (5)$$

,where ΔC is the concentration gradient across the membrane.
In **paper II**, the situation is more complex in comparison to the illustration in figure 7. Instead of loading/unloading of solutes, only release (unloading) of initially loaded vesicle content (catecholamines) is studied. The vesicles (LCDVs) contain catecholamines and nucleotides that are stored (bound to the dense core protein and in aggregates in the halo). Even though both kind of solutes (when unbound and not aggregated) are able to cross the vesicle membrane, conditions within the LCDVs needs to be changed in order for these storage vesicles to release their cargo. In the paper, partial release is observed when compressing/decompressing the vesicles as in **figure 8.2**, using sucrose which does not cross the membrane (at hours/days time scale).

3.2 Protein facilitated transport across the cell membrane

Although water, O_2/CO_2, and most of the important nutrients and waste can pass the cell membrane through simple diffusion, there also exists many specific dedicated transporter proteins, that increase transport rates across the membrane considerably (**fig.9**)[56]. Diffusion through the lipid bilayer, diffusion through a channel protein and transport along the osmotic gradient via a transporter protein are all modes of passive transport (no added energy needed). Passive water transport through channel proteins, for example aquaporins, is substantially faster than simple diffusion,[57] and could help cells to respond faster to osmotic stress. In contrast active transport, transporting molecules against the osmotic gradient, costs ATP (energy), however, active transport is necessary for the cell to maintain osmotic imbalances that in many cases are important for its function (**fig.9**).

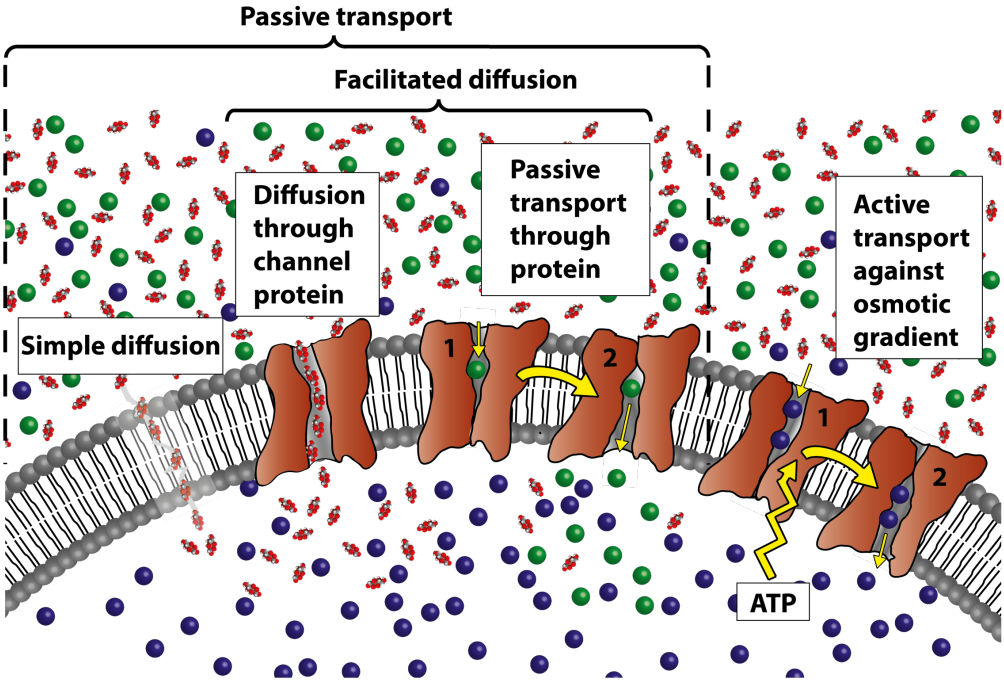

Fig.9 *Showing the different modes of transport. Sorbitol (red and white molecule) can diffuse through the lipid bilayer or through some special channel proteins. The green molecule however can only pass through a specific transport protein along the osmotic gradient. Passage through channel proteins and dedicated transporter proteins along the solute gradient is called facilitated diffusion. The blue molecule is also impermeable to the lipid membrane but is selectively pumped against the osmotic gradient using ATP.*

In the case of the chromaffin vesicles in **paper II**, their membranes are functionalized with H^+-ATPase, which with energy from ATP actively transports a proton H^+ across the vesicle membrane (**fig.10**). The surplus of protons are both used to keep an inside pH of 5.5, but it is also used to drive a number of active transporters like VMAT, that uses protons to pump dopamine outside the vesicles (cytosolic concentration of perhaps ~0.5 mM dopamine in the chromaffin cells),[58] into the vesicles with catecholamine concentrations at ~0.35-1 M (however, once inside the dopamine binds to the dense core or forms aggregates with nucleotides (ATP,ADP and AMP) for storage). The active transporter VNUT actively transports ATP into the LDCVs, where they are stored, both bound top the dense protein core and in aggregates in the cytosol at 150-300 mM concentration.

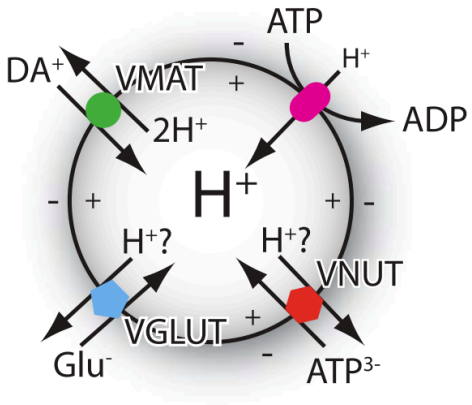

Fig.10 *Example of active transporters in chromaffin secretory vesicles. Illustration shows how H^+-ATPase with help of extravesicular ATP pumps protons into the LDCVs which is used to maintain pH 5.5 inside as well as subsequently driving dopamine accumulation through VMAT, suggestedly ATP through VNUT and glutamate through VGLUT (found in smaller sized chromaffin secretory vesicles without dense core). Image from* [17].

3.3 Model membranes

Often in studies of passive and active transport, simplified model membranes are used instead of cell membranes. One of the reasons for this is that there is no control over the number of transporters in the membrane of each vesicle derived from cell membranes. This makes it difficult to say something specific about some particular transporter protein. In some cases, there may also be present multiple types of transporters for the same solute in the cell membrane, glycerol for example could be transported both by glycerol transporters and by some different types of water transporters (aquaporins). Also in some cases there may be non-specific interactions between the solute and some molecules in the membrane.

As stated earlier, cell membranes have very complex compositions of lipids, proteins, glycoproteins and glycolipids. To perform studies directly on cell membranes, is commonly not possible when one wants to look at a single specific aspect or function of the cell membrane. To simplify the situation, researchers therefore often us simplified model membranes, commonly with single/simple lipid compositions, in a bottom-up approach. These model membranes could either be studied directly or by incorporating one or more types of proteins in order to study their function. Studying a simplified case, makes it possible to gain insights with higher certainty than for the more complex case; however, one must not forget that one also loses information about the role of complex intermolecular interactions for cell-membrane function To better understand how these model membranes look and which properties they have, we need to take a closer look at the characteristics of the lipid components and at the formation of lipid bilayers.

3.3.1 Lipids and Lipid bilayer formation

The most common type of lipids found in the cell membrane are phospholipids. As nearly all types of lipids they are amphipathic, which means that they consists of both hydrophilic (likes water) and hydrophobic (dislikes water) parts[23]. The headgroup is hydrophilic and the tail region is hydrophobic as exemplified below with the phospholipid 1-palmitoyl-2-oleoyl-sn-glycero-3-phosphatidylcholine (POPC, **fig.11**), which belongs to the most abundant type of phospholipids in eukaryotic cell membranes, phosphatidylcholines. Most types of lipids have 1-2 hydrocarbon tails

(but could have up to 4). The hydrocarbon tails could either be saturated or contain one or more unsatrated bonds (depicted by the kink on the right tail in **fig.11C**). The number of tails as well as the grade of unsaturation of the tails affects the lipids structure. The geometry of lipids with two tails is usually cylindrical in shape, while lipids with one tail have a more inverted cone like geometry (**fig.12,13**). Lipids with more than two tails or two tails with high unsaturation or two tails at high temperature tend to have a cone like geometry.

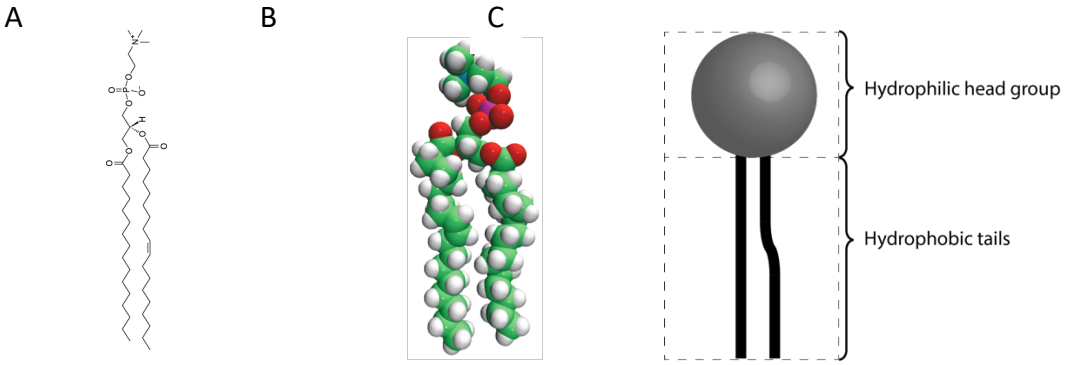

Fig. 11. *POPC (**a**) Chemical structure, (**b**) space-filling model and (**c**) simplified sketch. Images A and B are from* [59]*.*

The amphipathic nature of the lipids makes them, when in an aqueous environment, aggregate and self-assemble into different structures, the driving force being to mask the hydrophobic parts from the aqueous environment and in this way minimize the free energy of the system[23]. The minimization of free energy is here dominated by thermodynamic processes. All systems strive to maximize the entropy (increasing disorder), which is also the case for freely diffusing water and lipid molecules. When the hydrophobic parts of lipids are exposed to water, this forces the water molecules close to them to become ordered (which is entropically unfavorable). The drive of the water molecules to increase their entropy causes the lipids to self-assemble (aggregate) in ways that minimizes the exposed hydrophobic areas (similar to oil forming droplets in water). Lipids will self-assemble in ways that shield their hydrophobic parts the most, depending on their different geometries, two common assemblies are shown in **figure 13**. Israelachvili introduced the concept of a critical packing parameter (*cpp*),[60] which could be described as

$$cpp = \frac{v}{a_0 l_c} \tag{6}$$

, where v is the volume of the hydrocarbon chain/-s, a_0 is the optimal headgroup area (balancing the headgroup repulsion with hydrophobic attraction), and l_c is the length of the of the hydrocarbon tail (when packed),[61] see **fig. 12.**

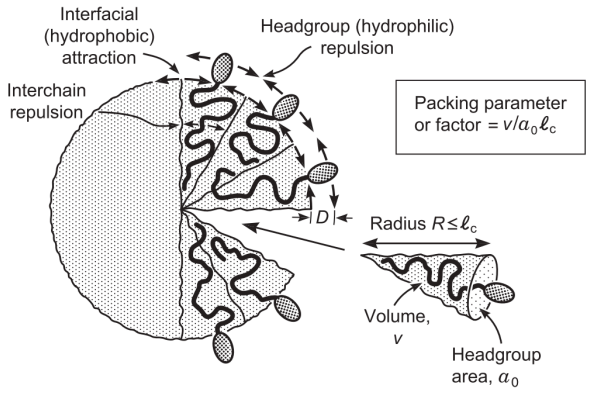

Fig.12. A geometrical description of the terms of the critical packing parameter. Image from Ref.[61].

The cpp geometries could be divided into inverted cone (cpp < 1/3), cylindrical (1/2 < cpp < 1), cone (cpp > 1).
The cpp could be used to predict what kind of self-assembly formation will be the result of hydrophilic/hydrophobic interactions for a lipid with a certain geometry (**fig.13**). Based on these geometrical cpp shapes of the lipids, some types of lipids with an inverted conical geometrical structure form micelles, while other types like the phospholipids with a more cylindrical cpp structure, used in this thesis, forms double layered lipid vesicles in an aqueous solution [23], see **fig. 13**. Further, the cpp geometry, suggests that lipids of a certain geometry would have an optimal average vesicle size (curvature) where the free energy would be at a minimum.

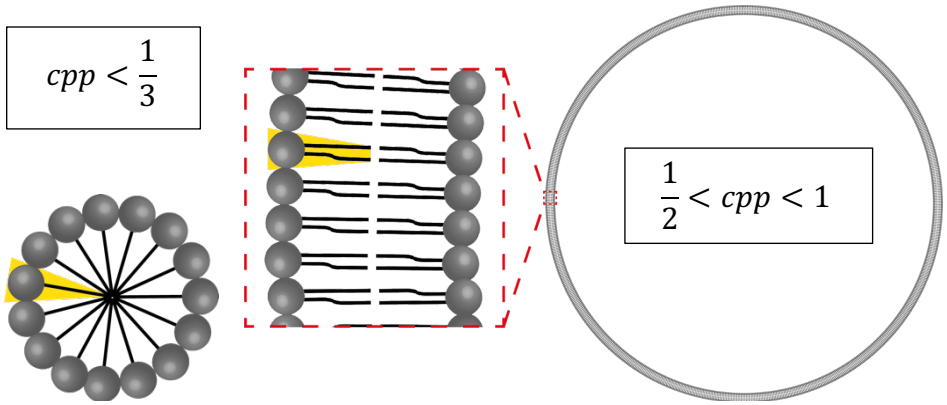

Fig. 13. *Self-assembly of lipids in water. Depending on the cpp of the lipids, different lipids form different types and sizes of structures, in order to shield their hydrophobic parts from water. Left panel: Sphingolipids, lipids with only one hydrocarbon fatty acid tail, forming a micelle. Right panel: Phospholipids, lipids with two hydrocarbon fatty acid tails, forming a bilayered lipid vesicle.*

Another important characteristic of lipids is their difference in melting temperature T_m (related to the grade of saturation of their hydrocarbon tails). Below the melting temperature, the lipids turns into a highly ordered gel-phase. At temperatures above T_m they melt and turn liquid. Vesicles with lipids at gel-phase temperatures have about an order of magnitude lower permeability compared to the vesicles with same lipids in fluid-phase. However, at temperatures close to T_m, the permeability could increase drastically, an explanation could be that some regions of lipids in the membrane are in gel-phase while others regions are in fluid-phase, this could create transient pores in the membrane [62–64]. The grade of saturation and lipid composition too affects the lateral fluidity of formed bilayers,[65,66] and most physiological lipids are in fluid phase at body temperature, providing the cell membrane with its lateral fluidity. The sterol lipid

cholesterol, present at high concentrations in the cell membrane and in LDCVs, also serves to increase the order in the membrane, packing the hydrocarbon tails tighter by filling out gaps in between. In this way, increasing levels of cholesterol in the lipid bilayer, results in increasing stiffness and lowered permeability The fluidity of the cell membrane at physiological temperatures provides it with a flexibility that is used in many important cell functions.

3.3.2 Biophysical properties of lipid membranes

Below follows a description of the ways in which lipid membranes can deform and some examples of how these deformations connect to different cell functions.

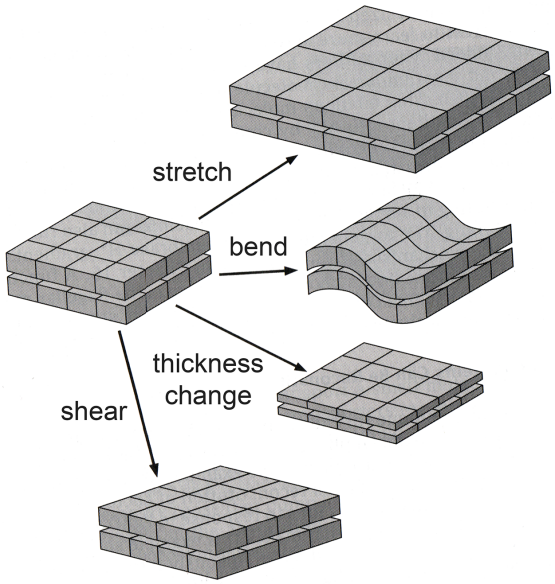

Fig.14. *Showing the different types of lipid membrane deformation. Image from Ref.*[26]

Membrane bending (**fig.14**) is for example needed for vesicle fusion to the cell membrane during exocytosis (**fig.3c and 15a**),[67] as the isolated chromaffin vesicles, in **paper II**, would naturally do if they still resided within the chromaffin cell. Membrane bending is also essential for vesiculation and vesicle encapsulation during endocytosis. Lipid membranes of various compositions have different membrane flexibility. The flexibility is determined by a membrane's *bending stiffness*, which is a parameter that describes how much force is needed to go from a resting membrane state to a locally extruded shape. The bending stiffness is typically measured by pulling out a nanotube from a vesicle with optical tweezers[68]. Interestingly, it has been found that cells use similar nanotubes for communicating with surrounding cells in its close proximity [44]. Membrane bending is costly, but, as all these modes of communication via exocytosis, endocytosis and nanotubes are common for the cell, the cell membrane in itself is functionalized with means of reducing this cost. One way the cost is reduced is by migration of lipids. Within the cell membrane are a large variety of lipids (~1000) with different cpp geometry (see **section 2.2.1**). Lipids preferring high curvature migrates towards and are enriched in areas with high membrane bending (as it is more energetically favorable for them to reside there), this drastically reduce the bending cost [69,70]. There are also curvature inducing proteins, like clathrin and snare proteins, that together with other proteins induce formation of vesicles during endocytosis [71]. For our purpose in **paper I**, we could see the relatively high bending cost as something positive. For the vesicles with the larger size range, we used a high concentration (69%) of a lipid (DMPC) which has a T_m at 24°C [72]. So, the vesicles, although likely not in gel-phase (due to the addition of the

other lipids in the composition), would have a relatively high bending stiffness at room temperature ~21°C. This means, that the vesicles' relatively high stiffness would make them less prone to deform as they adsorb to a surface (from possible interactions with the surface). If vesicles were deformed at adsorption, larger sized ones would tend to deform more than smaller ones (smaller vesicles are typically stiffer and larger ones have a larger surface area in close proximity to the surface, which could lead to more interactions). In case of such deformations, where larger vesicles deform more, the deformed vesicles would show a higher intensity than expected and introduce an error in the fluorescence to size conversions.

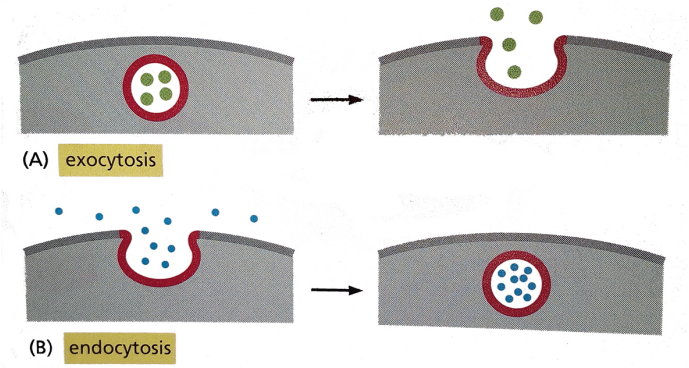

Fig 15. *(**a**) Showing vesicle membrane bending and fusing with the cell membrane during exocytosis. (**b**) Internalization and budding off vesicle during endocytosis. Image from Ref.* [23]

An example of *membrane stretching* is when vesicles or cells swell during hypoosmotic shock. The osmotic force acting on the membrane, simultaneously acts to draw membrane components apart in order to increase the volume. This as a means of balancing the osmotic gradient across the membrane. As mentioned earlier, in section 3.1.1, the energetic cost of membrane stretching far exceeds the inside pressure caused by the osmotic gradient across the membrane, and thus osmotic equilibrium is not achieved.

Shearing is when the two leaflets of the bilayer moves independently of each other. One example of this is shear-driven SLBs where the lower leaflet stays stationary while the top leaflet, by flow induced force, moves over the front edge in a rolling motion (in a motion similar to the one of the driving belts of a tank)[73]. There is an energy cost associated with shear-driven motion as there is friction between the bilayers, also any presence of transintegral proteins serves to increase the friction further.

Lateral compression could for example be when a transintegral membrane protein is incorporated where the hydrophobic region of the protein does not match the membrane thickness. In absence of lipids with matching length of their hydrophobic tails present, the tails of the lipids are either stretched or compressed to match the length of the hydrophobic region of the protein.[74]
All these manipulations of the lipid membrane from its lowest energy state requires energy input to be accomplished. For membrane deformations that are commonly used by the cell, there exists various means of reducing the associated energy cost. However, this is often not the case for simplified model system such as lipid vesicles.

3.3.3 Preparation of unilamellar liposomes

There are many ways to prepare synthetic lipid vesicles, many of which being described in a review by Szoka et al. [75]. Perhaps the most common technique to prepare vesicles is to mix lipids in an organic solvent, usually chloroform, dry the solution under nitrogen while rotating the flask to make a thin lipid film. The flask is then put under vacuum for > 1-2h to remove all traces of organic solvent. When hydrating this film, the vast majority of the vesicles become multilamellar (MLVs), consisting of several layers of vesicles with decreasing size inside one another. In most experiments, it is desirable to have one-layered vesicles. This is also the case when using lipid vesicles as drug carriers as the unilamellarity increase the loading efficiency. Likewise, for experiments like those conducted in **paper I**, where we correlate vesicle fluorescence intensity with vesicle size, it is highly desirable that the vesicles are unilamellar (contain only one bilayer), as vesicle intensity for a vesicle with multiple layers would look like a much larger vesicle than it actually is. In our experiments, this could lead to an overestimate of the number of large sized vesicles. Fortunately, there are some ways to reduce this risk. One way to ensure a higher level of unilamellarity, is to freeze-thaw the vesicle solution (freezing in liquid N_2 and then thawing in a 55°C water bath for ten cycles). This is known both to increase vesicle loading and unilamellarity.[76,77] Another common technique of reducing multilamellarity and homogenize vesicle size distributions is to extrude the vesicle solution through a porous membrane, in our group we've found that extrusion back and forward about 31 times is optimal (unpublished finding). [78,79]

3.3.4 Common lipid based model systems

Bangham et al. first discovered liposomes in 1960's.[2] They have since been used for a multitude of things including cell membrane models to study molecular interactions [80] and for studying membrane incorporated proteins [31,81,82], models for measuring membrane permeability[2,51,83–89] and for being used as drug carriers[90] with high targeting specificity[91,92]. The terms liposome or vesicle has many times been used interchangeably, but vesicles could in some cases be formed with other building blocks than lipids.

As previously mentioned, native cell membranes offer a many times too complex environments to be certain that the measurement signal stem from one single aspect or function to be studied, for this purpose a simplified model is often preferred. The most common membrane models are lipid vesicles (also called liposomes, **fig.17**) and *supported lipid bilayers* (SLBs, **fig.16c**), both commonly with single lipid composition or containing only a few types of lipids. SLBs could be formed by letting small vesicles adsorb to a thoroughly cleaned SiO_2 or TiO_2 surface. At a high enough surface coverage, the vesicles will start to burst and form a SLB (this is energetically favorable as it provides better shielding of the hydrophobic parts).

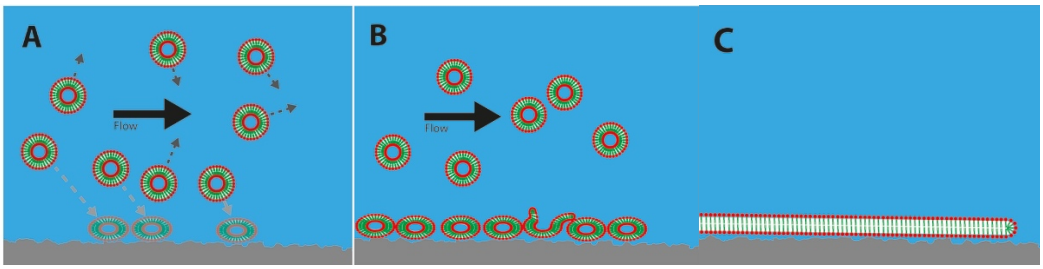

Fig.16. *(**a**) Flow of vesicles which at the same time diffuse, resulting in that some reach and adsorb to the surface where they flatten slightly (not to scale) (**b**) Vesicles start to rupture in a chain reaction at a critical concentration on the surface. (**c**) A supported lipid bilayer is formed from the ruptured vesicles.*

SLBs have the advantage of bringing the molecular interactions studies in very close proximity to the sensor surface, which boosts the signal intensity of surface sensitive techniques such as TIRF-microscopy and SPR (with SiO_2 covered surface). SLBs are excellent for checking aspects such as diffusivity of membrane incorporated components by FRAP. SLBs are also good to look at molecular interactions between SLB incorporated receptors with a fluorescently labelled ligand, or ligands attached to fluorescently labelled vesicles. They can also be driven by a shear flow as a means of enriching labelled molecules at the front of the bilayer[93]. It have also been proposed as a model to be used for 2D diffusional size determination of membrane attached nanoparticles[94]. The short distance between the bottom lipid leaflet to the surface, about 1 nm, could also be a disadvantage as this small gap could, for example, affect transintegral membrane proteins lateral mobility and function. As a solution to this particular problem, SLBs have been formed with the bottom leaflet resting on incorporated PEG-cushions, increasing the distance between the bilayer and the surface.[74]

As, stated before (in section **2.2.2**), the large variety of lipids present in the lipid membrane fills different purposes, one being to reduce the cost of membrane bending. In several ways, vesicles based on complex lipid compositions also, apart from providing a more natural lipid environment, share more of the physical character of the cell membrane compared to single/few lipid compositions. A more natural lipid composition is also preferable when reconstituting membrane proteins into membranes, as doing so with a single lipid mixture or a composition too different from the protein's native environment, could cause the protein to denature (misfold, by hydrophilic-hydrophobic mismatch) and stop working. To reduce this risk, it is preferable to use a composition that is as close to the protein's native environment as possible. Lipid compositions that more closely resemble natural compositions, could be made from lipid extracts from, for example, E.coli, soy, brain and yeast.

Vesicles are the preferred method of studying membrane permeability. SLBs are useful for looking at lateral diffusion within the lipid bilayer using FRAP, or at molecular interactions between surface attached molecules with FRET. SLBs are also useful in making the sensor surface inert (decreasing solute adsorption and non-specific interaction with the sensor surface).

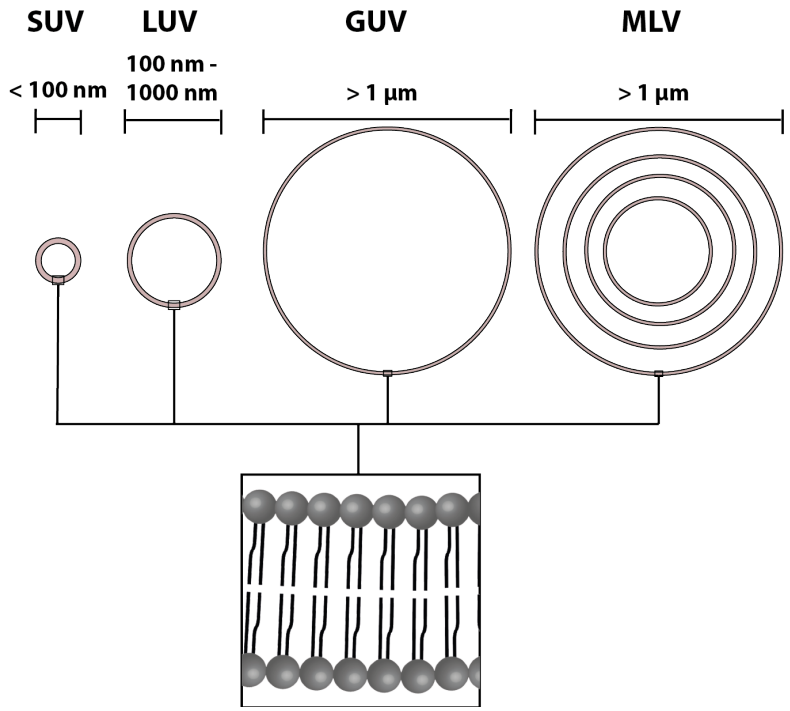

Fig.17. *The most common types of lipid vesicle models. Image modified from Ref.*[95]

Unilamellar vesicles (containing a single lipid bilayer), could be divided into three subcategories depending on size, small unilamellar vesicles (SUV) <100 nm, large unilamellar vesicles (LUV) ~100-1000 nm and giant unilamellar vesicles (GUV) ~1-10 µm [92,95,96] (**fig.17**). SUVs or small sized LUVs are preferred in use with surface sensitive measurement techniques, as the majority of the signals from these techniques typically are obtained within 150 nm of the sensor surface. The downside to these smaller vesicle models are that the curvature is a lot higher than it would generally be in the cell membrane. GUVs on the other hand has a size comparable with cells and is thus a better model in this respect. Extruded LUVs in some cases have been shown to form ellipsoid vesicles that turns more spherical over time in storage (>9 days) [97], while sonicated ones are more spherical to begin with. GUVs with single/simple lipid composition more easily lyse (burst) during osmotic stress [98]. So, choosing vesicle size is a tradeoff, with smaller vesicles giving high/detectable signals in surface sensitive techniques while being further in physical properties from the native cell membrane.

3.3.5 Lipid vesicles in surface based sensing

The main lipid based models used for studies in this thesis are based on smaller sized vesicles (SUVs and LUVs), attached to or interacting with a surface, in use with highly sensitive techniques.

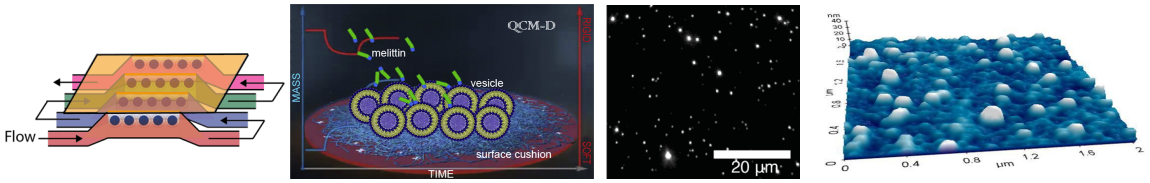

Fig.18 *Examples of vesicles in surface sensitive techniques. (**a**) SPR, four channels with immobilized chromaffin vesicles (**paper I,** not to scale), (**b**) QCM-D (not to scale, image from Ref.*[99]*), (**c**) TIRF*

*microscopy, immobilized vesicles of various sizes, in **paper II** and (**d**) contactless AFM of immobilized vesicles (image from Ref.*[100]*)*

3.3.5.1 Applications of vesicles at surfaces

There could be numerous possible applications of vesicles at surfaces. Also, most applications of vesicle studies that previously have been performed in bulk could also be studied with surface sensitive techniques, with higher sensitivities and reduced sample consumptions. Below are listed some different application areas for immobilized lipid vesicles.

Biosensor applications. Functionalized vesicles immobilized on surfaces or used in a sandwich assays could serve as a biosensor, many examples are given in reviews[5,101]. This could be to detect and resolve binding kinetics of cholera toxin [102]. Another example is virus detection[103], in this case (*norovirus*) in TIRF using fluorescently labeled functionalized vesicles.

*Molecular interaction*s and binding kinetics (binding rate/dissociation rate/ residence time). This could for example be to study *pharmaceutical molecules* affinity to their *target receptors.*[104] Lipid vesicles offer a natural environment for incorporating the target receptors which are usually some membrane protein, and the ligands could be attached to the sensor surface. Additionally, the vesicles in themselves serves to amplify the binding signal, as in this example where the already very sensitive signal of ligand-receptor binding signal was amplified ~23 times in SPR, by attaching the ligand to vesicles with high refractive index.[105] In many cases, especially in fluorescence microscopy, the vesicles even serve to make the signal detectable at all.[103,106]
Characterization of lipid vesicle properties such as size, membrane permeability of either synthetic ones like medicinal liposomes, to study binding affinity to target receptor/-s and time for release of cargo. Or naturally occurring vesicles like different types of exosomes [107–109], and chromaffin vesicles as in **paper II**. Also to study lipid membrane permeability, of vesicles with various lipid compositions, to different solutes. This could be done either directly by probing the changes in refractive index of the interior volume of surface attached lipid vesicles using SPR [31,110] or indirectly by monitoring the volume changes of vesicles during solute loading[111] (possible as vesicles during hyperosmotic shock and volume recovery during solute loading act as perfect osmometers).

Improved understanding of cellular components and function.
By incorporating membrane proteins into lipid vesicles (*proteoliposomes*), it is possible to study *protein functionality*.[31] This could either be done for a single type of protein or for a group of interdependent proteins to study their cooperative function. Further, it has also been studied how membrane protein function may be affected by curvature induced strain when incorporating is done in different sized vesicles.[82] *Enzymatic activity*, vesicles could either enclose/incorporate enzymes or study interaction between enzymes in bulk and surface attached vesicles [112]. Vesicles have also been used to obtain a better understanding of exocytosis/endocytosis as in this example of a *vesicle fusion assay*[113].

More examples of applications of vesicles at surfaces in surface sensitive techniques could be found in reviews.[5,114]

3.3.5.2 What is to be gained by studying vesicles at surfaces?

Many examples of the benefits of studying vesicles at surfaces were already presented under the section *applications of vesicles at surfaces* (3.2.5.1). Here instead we focus on the more technical/practical gains of studying vesicles at surfaces.

Sensitivity

The first main advantages of attaching vesicles at a surface are to be able to use these cell membrane models with highly sensitive surface based sensing techniques, significantly boosting the signals of whatever interaction is to be studied (a 10000 times improvement in signal strength was seen in SPR, Ref.[80]). SPR is already a sensitive technique and can detect as little as 1 pg/mm^2 (**fig.18a**) adsorbing to the sensor surface, while quartz crystal microbalance with dissipation (QCM-D) has a sensitivity of 1 ng/cm^2 with the added opportunity to monitor changes in dissipation of the signal which makes it possible to probe structural changes (i.e. increased/decreased rigidity of the adsorbed film) (**fig.18b**). In contrast to these two ensemble techniques, TIRF microscopy can probe individual vesicles and has been used for single molecule detection (**fig.18c**), and atomic force microscopy (AFM) has a nanometer spatial resolution and could be used to probe the 3D geometrical structures at the surface (however, as vesicles are soft, contact versions of AFM may lead to vesicle deformations) (**fig.18d**).

Incorporated flow system enabling high throughput screening and possible miniaturization

The other main advantage of using surface sensitive techniques is that most of them are compatible with flow systems. This makes it possible to easily change the solution surrounding the immobilized vesicles, and in this way allowing for more complex and also repeated studies on the same set of vesicles. This opens up for possible high throughput applications, like drug screening. Even more advantageous are microfluidic fluid systems, which offers extremely low sample consumption and supreme control by the laminarity of the flow (one directional flow - no turbulence) occurring in channels with height and width lengths typically in the range of hundreds of μm. The narrow dimensions means that all of the solution is flowed very close to the sensor surface, making adsorption very effective due to very short diffusional distances. More effective interactions/adsorptions means that less material is needed apart from the sheer miniaturization of volumes.

Parallelization enabling high throughput measurements

In SPR, it is also possible to perform several measurements at once, as depending on the make, an SPR instrument could have several parallel flow channels (with interconnected flow) on the same sensor chip, this could give very time-efficient measurements, as it means that it is possible to perform many experiments at the same time (**fig.18a**). In TIRF one could also perform simultaneous measurements as one could attach different types of vesicles, which could be made distinguishable by applying different fluorescent labels, or one could study different sizes of vesicles at the same time, by correlating size with intensity as we do in **paper I** (**fig.18c**).

3.3.5.3 Surface modifications and tethering strategies

The idea of surface modification in our case is to immobilize vesicles as close to the surface as possible to enhance signal out while at the same time keeping the vesicle far enough from the surface to prevent vesicle surface interaction. Any direct surface interaction between vesicles

and surface, would likely cause the vesicles to deform. Any deformation would affect vesicle volume and any calculations and conclusions drawn based on the assumption that the adsorbed vesicles are spherical. Another key aspect of surface modification in regards to surface sensitive techniques is to prevent non-specific binding between the solutes in the bulk solution with the sensor surface, as this would produce an unwanted signal response that in most cases would interfere (superimpose) with the signal coming from the interaction to be studied, and skew the measurement outcome and conclusions.
There are a number of commonly used commercial first step surface modifications available: PLL-g-PEG/PLL-g-PEGBiotin (for SiO2), dsOEG/dsOEGBiotin (for Au), bovine serum albumin BSA/BSA-Biotin, Streptavidin/NeutrAvidin. It is also possible to use a SLBs with incorporated biotinylated lipids as a first step (on SiO2/TiO2).
A SLB modification is considered most inert to non-specific solute binding is a SLB, but to form an intact one requires extremely clean SiO2 or TiO2 surfaces, also things attached to SLBs generally diffuse (unless in gelphase or by mixing in a high conc. of biotinylated lipids ≥5 mol% and then saturating with SA/NA).

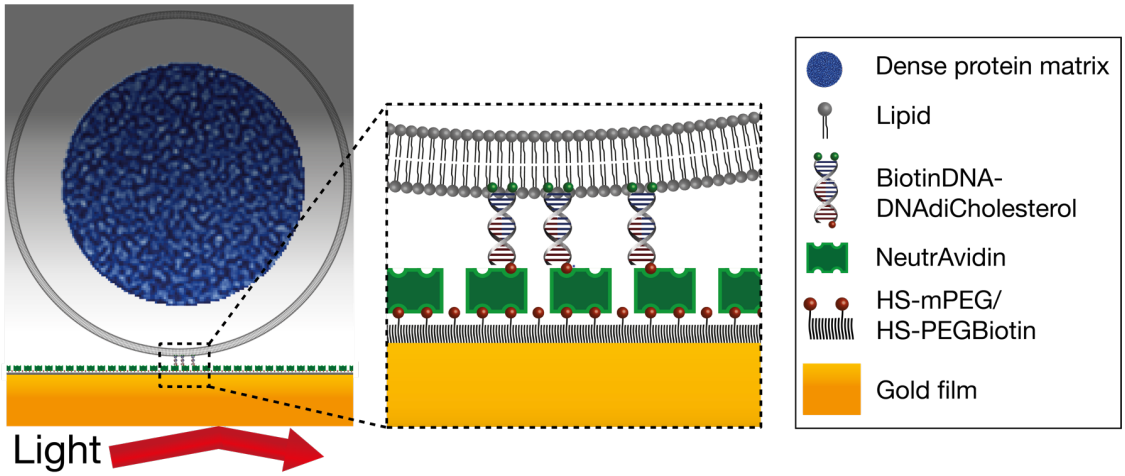

Fig.19 *Pictogram of a large dense protein core vesicle, attached to a functionalized SPR sensor chip with a DNA-linker. The short linkers and surface modifications puts the vesicles at a ~15 nm distance from the sensor surface, which means that about half of each vesicle is within the sensing depth* δ *~ 150 nm.*

On top of all biotinylated modifications, it is possible to attach SA or NA as a bridging step, the biotin-streptavidin coupling is one of the strongest non-covalent coupling known in nature ($K_D \approx 10^{-15}$ M)[115]. Vesicles with some linker biotinylated at the end could then be attached as a next step.
The linker could, for example, be a DNA-linker as shown in **fig.19**, which is very convenient when working with natural vesicles (exosomes, LDCVs) or vesicles derived from isolated cell membranes, as the linker can be added to the vesicles by incubation. For synthetic vesicles, it is possible to add linkers directly by mixing in a fraction of biotinylated lipids into the lipid composition (**fig.20**). When adding linkers, it is important keep the number of linkers per vesicle down to about ≤ 10, as a large number of linkers (given enough attachment points on the surface), would cause the vesicles to deform upon adsorption. For natural vesicles, the concentration of vesicles could be estimated with NTA, it is then possible to add DNA-linkers in a perhaps 5:1 (linker/vesicle) ratio. For synthetic vesicles, it is necessary to roughly know the vesicle size distribution after extrusion, to be able to calculate what fraction of biotinylated lipids to add into the composition to give the desired number of linkers per vesicle.

Another design parameter that could be used, especially for measurements in TIRFM where it is important to keep vesicles at a distance from each other in order not to risk confusing a number of small vesicles for one larger, is to constrain the number of anchoring points on the surface. In **paper I**, we choose a ratio of 10000:1 for PLL-g-PEG and PLL-g-PEGBiotin, which gave a surface density of ~2 biotins per um^2. This is also a way to control the number of surface attachment points, which here comes to ~1 attachment per vesicle even for larger ones.

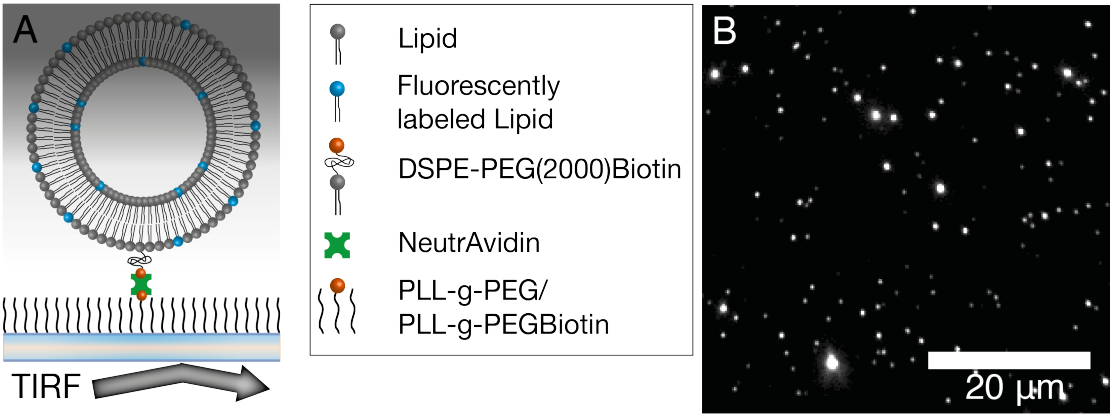

Fig.20. *(**a**) Pictogram of a surface attached vesicle in **paper I** (not to scale). The image shows the surface modification and the coupling strategy used and hints at the from the surface exponentially decaying sensing field. (**b**) A micrograph of the attached fluorescing vesicles in TIRF microscopy.*

We have now looked at some benefits and considerations of using lipid vesicles in surface based sensing and will now look closer at some of the sensing techniques mentioned throughout the thesis.

3.3.5.4 Our examples of vesicles at surfaces

In **paper I**, we adsorbed vesicles, with incorporated fluorophore headgroup-labelled lipids, to a functionalized glass surface in TIRF microscopy. TIRF microscopy allows individual vesicles to be studied (**fig.20b**). We could then correlate the recorded distribution in fluorescence intensity of all vesicles, to the vesicle size distribution of the same vesicle batch probed in Nanosight tracking analysis. Knowing the individual sizes of vesicles on the surface in TIRF allows, for example, studies looking at membrane curvature (vesicle size) dependence for the function of membrane incorporated proteins.
In **paper II**, we study chromaffin vesicles adsorbed to a SPR surface (**fig.19**). This allows for direct screening of any changes in refractive index of the adsorbed vesicles over time, i.e. to study if the chromaffin vesicles have been able to keep their initial catecholamine loading during isolation and purification steps, by stimulating catecholamine release. Studying the chromaffin vesicles in SPR, also allowed for us to characterize the hydration level of the dense core, in a new approach, by exchanging similar buffers based on water/heavy water, before and after vesicle adsorption.

4 Methods

Here follows an introduction to the techniques used in **paper I** and **II**. It starts off with a more thorough look at TIRF and SPR, the main methods used. Then follows a short description of amperometry, an electrochemical technique used in **paper II**. Last follows shorter descriptions of three different techniques for determining vesicle sizes.

4.1 Microscopy

As briefly mentioned in the beginning of the thesis, microscopy was first developed in the 17th century by van Leeuwenhoek and Hooke[116]. A lot has happened since then, especially in recent years, with an explosion of new types of microscopy techniques. Ever since Hooke's first observations of the cell came to revolutionize our understanding of biological life, improved microscopy techniques continues to offer new platforms enabling new discoveries.

4.1.1 Fluorescence and Fluorescence microscopy

For conventional optical microscopy, the smallest separations between objects that enable them to be individually observed is around 200-250 nm in size due to the diffraction limit *d* [117], which could be described as

$$d \approx \frac{\lambda}{2NA} \tag{7}$$

, where λ is the wavelength of the incident light and *NA* the numerical aperture of the objective (*NA*=1.49 was used in **paper I**). However, if separated further apart than this, smaller objects can be identified on an individual level, given that their optical contrast is sufficiently high. One way of increasing the optical contrast between and object and its surrounding is by attaching fluorescent molecules. In this way, individual nm-sized objects like proteins, antibodies and liposomes that would otherwise be difficult to observe can be observed.

Figure 21 shows a Jablonski diagram which represents a simplified description of a fluorophore absorbing an excitation photon and emitting a lower energy photon, where lower energy means that the emitted photon will have a longer wavelength than the one of the exciting photon. As the exciting light has a shorter wavelength than the emitted light, it is possible to use an emission filter to only observe the emitted fluorescence (**fig.24**).

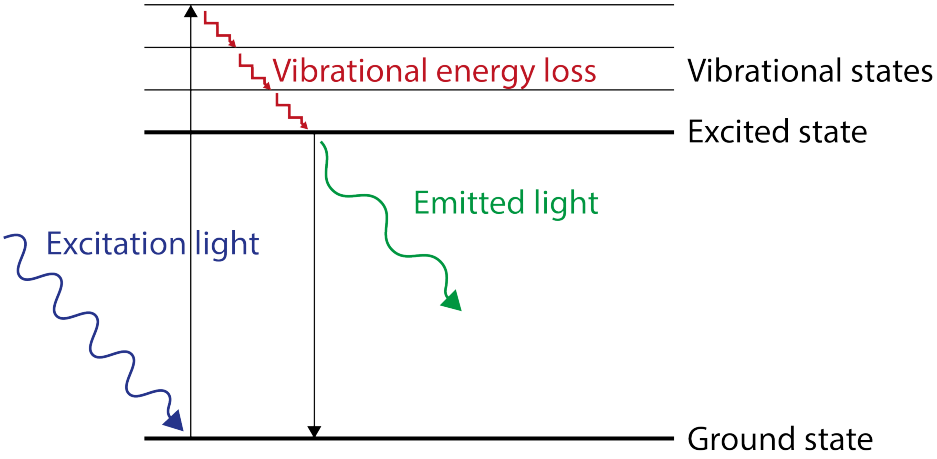

Fig.21 *Jablonski diagram gives a simplified description of how an electron of a fluorophore adsorbs a photon that brings it to an excited state; upon returning to the ground state it emits light of a longer wavelength.*

Figure 22 shows an excitation and emission spectrum for the particular fluorophore used in **paper I**. With the inserted color bar we can see at what color the dye is excited and what color light it emits. The distance between the excitation and emission peaks is called the Stoke's shift, a small Stoke's shift makes a fluorophore more prone to self-quenching and vice versa.

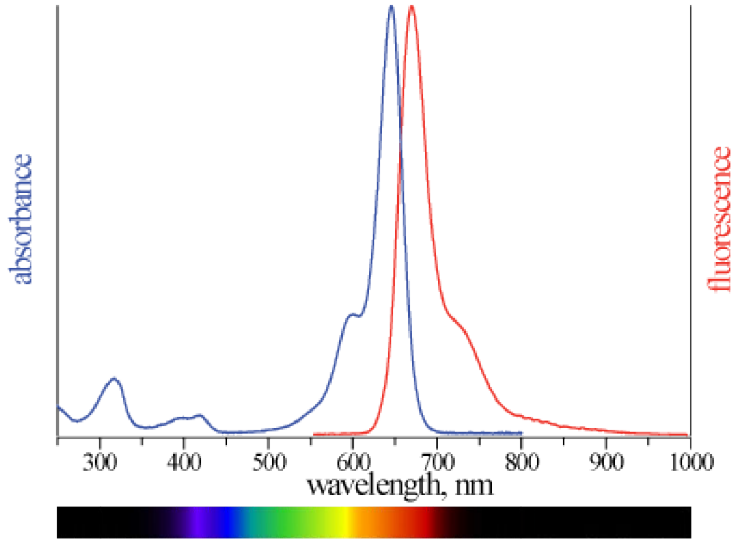

Fig.22 *Excitation (absorbance) and emission (fluorescence) spectrum for Atto-647N dye used in* ***paper I****. Excitation is achieved, at its peak, by orange/red light, while the emitted light is deep red. Image adapted from Ref.*[118]

Fluorescently labeled molecules are often commercially available, and if the molecule of interest is not available there are several protocols to covalently attach fluorphores to the molecules of interest. For lipids, both head-group and tail attached fluorophores exists. When labeling synthetically made vesicles, typically ~1% fluorescently labeled lipids are mixed into the lipid composition. In **paper I**. Some types of fluorophores are water soluble and are used free in solution, while some others are slightly hydrophobic and could be inserted into for example biological membranes by incubation. There are also genetic modifications inserted into the genome of some species or added as a plasmid (gene inserted into the cytoplasm of a cell), that often is made to overexpress a green fluorescent protein (GFP, also other versions available). The

overexpression of the fluorescent protein in all cells turns the whole organism fluorescent. There are many applications of fluorescence, apart from being used only for visualization of some molecules in microscopy. The water-soluble dye calcein has been added inside vesicles to monitor permeability indirectly, as changes in vesicle volume during loading of solutes (by working at its linear regime of concentration dependent fluorescence self-quenching) [111]. Some other fluorphores like carboxyfluorescein are pH sensitive and could be encapsulated into vesicles to follow changes in pH inside of these. In other cases two different fluorophores are used, the first with an emission spectra that overlaps the excitation spectra of the other. By attaching these to two molecules, between which interactions are of interest, it is possible to only use excitation light that will excite the first fluorophore. However, during interaction between the two types of molecules, the fluorophores are brought close enough to one another to allow for direct emissionless fluorescence resonance energy transfer (FRET), from the excited fluorophore directly to the other type of fluorophore which goes on emitting light of a longer wavelength. Now light of that wavelength only exist at points of colocalization between the molecules of interest. There are also fluorescently labeled antibodies made to target some receptor, and other specifically targeting labeled molecules. There are very many other uses of fluorophores [119].
With this basic understanding of fluorescence and the use of some fluorophores, we will now look closer at a commonly used fluorescence microscopy technique.

4.1.2 TIRF Microscopy

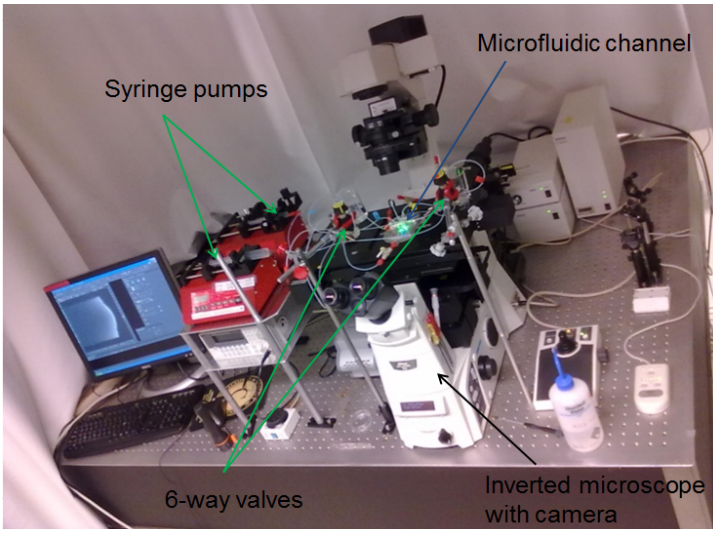

Fig.23. *Inverted fluorescence microscope Nikon Eclipse Ti-E, equipped with an EM-CCD camera, a mercury lamp light source connected with a fiberoptic cable and a 60x oil immersion TIRF objective. In the experiment in the picture, a microfluidic channel is mounted and connected with tubing to two 6-way valves that direct which flow paths in the microfluidic chip are used. The flow rate is controlled by two syringe pumps.*

One of the more potent fluorescence microscopy techniques is total internal reflection fluorescence microscopy (TIRFM). The main benefits of the technique are to be able to illuminate fluorophores along the substrate within a thin slice up to 150 nm from the surface, which significantly reduces out of focus fluorescence, thereby dramatically improving the signal to noise ratio. This makes it possible to observe interactions of surface attached molecules without the disturbance from the bulk solution above the substrate. Total internal reflection (TIR) occurs when the excitation light hits the SiO_2 surface at an angle higher than the critical angle ϑ_C, above which all light is reflected (**fig.25**). As the light is reflected, planar evanescent waves are created

in close proximity to and parallel to the SiO_2 surface. The intensity of this field has typically a decay length $\delta \approx 150$ nm. In this way the incident light photons are able to interact and excite fluorophores close to the sensor surface. Total internal reflection resulting in planar evanescent waves, fluorescence and microscopy was first combined and used in TIRF microscopy by Axelrod [120].

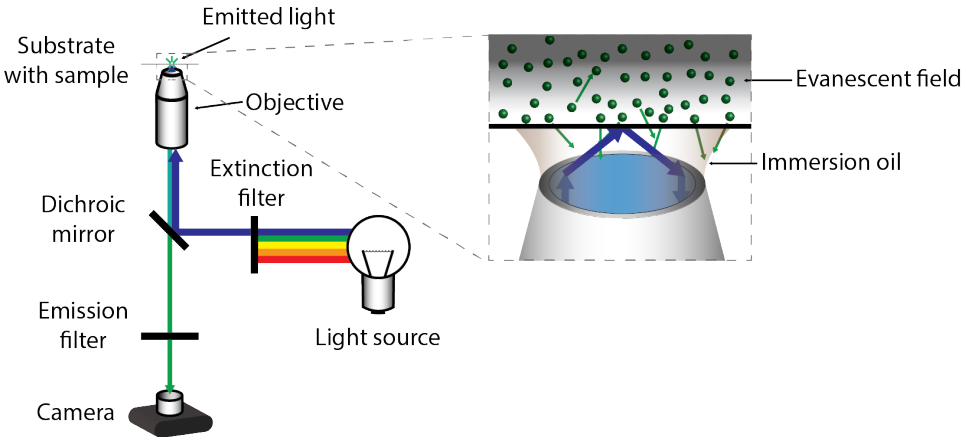

Fig.24. *Sketch of a TIRF microscopy setup. Light from a light source is passed through an extinction filter, and lead up through the objective onto the back of a thin glass slide, at an angle where it is totally internally reflected. The reflection of the excitation light causes an evanescent wave to occur in close proximity to the glass slide surface (portrayed by the gradient in the closeup). Some of the fluorescently labeled molecules sit close enough to the surface to have their fluorophores excited by the evanescent field. All light emitted in the direction of the objective is then collected and lead past a dichroic mirror, which reflects light from a certain direction (from the light source), while letting through light coming from the direction of the objective. An emission filter then removes the reflected excitation light and background light (of wavelengths different from the emitted light), leaving in principle only the light emitted from the sample.*

To better understand TIRFM, we need to take a closer look at the underlying theory.

4.1.2.1 Principles of Total internal reflection (TIR)

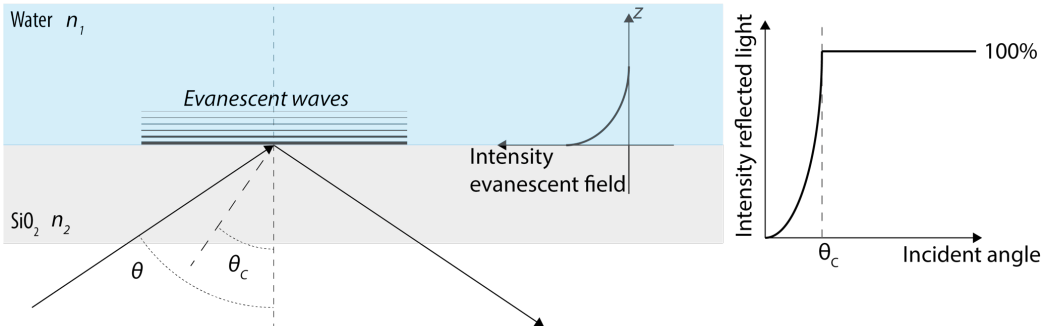

Fig.25. *Left panel: For light traveling through a media with refractive index $n_2 > n_1$ and at angles ϑ above a critical angle ϑ_C, all incident light is reflected at the interface. As the light is reflected, it causes planar evanescent waves to occur. Right hand inset shows how the intensity of the evanescent field decay exponentially with distance z from the interface. Right panel: For angles ϑ from 0° up to ϑ_c an increasing portion of the incident light is reflected, for angles $\vartheta > \vartheta_c$ all light is reflected (100% of the incoming intensity).*

As light passes through a medium with refractive index n_2 towards a medium with refractive index n_1, where $n_2 > n_1$, at angles ϑ larger than a critical angle ϑ_c, total internal reflection occurs. The critical angle ϑ_c is defined as

$$\theta_c = \sin^{-1}(\frac{n_1}{n_2}) \quad (8)$$

As this TIR occurs evanescent waves propagate from the point of intersection between the two medias. The intensity of the exponentially decaying evanescent field could be described as,

$$I(z) = I(0)e^{-z/\delta} \quad (9)$$

, where *I(z)* is the intensity at distance *z* from the surface and δ is the penetration depth of the evanescent field. The intensity at the penetration depth is given by Eq.5 as $e^{-\delta/\delta}=e^{-1} \approx 36.8$ % of the initial intensity. The penetration depth is determined by the wavelength of incoming/reflected light, the refractive index of the medium and the angle of incidence, as

$$\delta = \frac{\lambda_0}{4\pi n_2}(\sin^2\theta - \sin^2\theta_c)^{-1/2} \quad (10)$$

, where λ_0 is the wavelength of the incident light in vacuum.

One of the benefits of TIRFM, is the ability to discern heterogeneities in the sample by being able to study fluorescently labelled molecules separately (offering single molecule resolution if separated well enough). Depending on the field of view at the desired magnification around 1000 vesicles can be observed simultaneously per frame, because the vesicles need to sit far apart enough for each vesicle to be recognized as a separate vesicle (see e.g. **paper I**). This gives rather low statistics in comparison to ensemble measurements like in SPR measurements in **paper II,** where signal originates from about 10^5 chromaffin vesicles.

4.1.2.2 Experimental considerations

Handling of the images acquired is often conveniently done in ImageJ or processed in MATLAB scripts. There is usually uneven illumination across the field of view that needs to be taken into account and removed. This can be done by acquiring a number of background images (~10), taking the median value of each pixel position through the stack of images, then normalize the resulting image to the mean pixel value. To remove the uneven illumination from the experimental recording, divide each frame with the normalized median image.

4.1.2.3 Photobleaching

All fluorescence techniques suffers from photobleaching. Every time a fluorophore is excited, there is a small chance that it will not follow the ordinary excitation/emission path but end up in a state from which it cannot return to the ground state (often caused by oxidation), thereby the fluorophore stops fluorescing (is bleached). At high intensity incident light, the number of excitation/emission cycles are greater and photobleaching is more rapid. Some fluorophores are more resilient to bleaching like rhodamine, Alexa Fluor 448 and Atto-647N, other fluorophores like calcein bleach at a fairly high rate.

Photobleaching becomes a problem as soon as there is an interest in how fluorescence changes over time, for example, for a surface attached vesicle. To remove photobleaching from the fluorescence signal, a number of pre-measurement images are taken of the vesicles (~10) with the same settings that will be used in the rest of the experiment. A better estimate of the bleaching can be obtained by adding the last frames in the experiment (as baseline). Now it is possible to fit the decay vs. time or frame-number with a single exponential decay, with rate constant k (on the form $A \cdot e^{-k \cdot t} + C$), for either each vesicle or a bit less correctly (but less cumbersome) for the total intensity of all vesicles. We obtain the photobleaching as

$$Photobleaching(t) = A \cdot e^{-kt} \quad (11)$$

, where A is the initial amplitude of the fluorescence intensity.
Removing the bleaching from the experimental frames could then be done as

$$I_{corrected}(t) = I_{measured}(t)/Photobleaching(t) \quad (12)$$

With the photobleaching removed, it is possible to more accurately follow changes in intensity over time.

4.1.2.4 Some applications:

As mentioned above, this TIRFM lends itself to study surface interactions, or interactions in close proximity to the surface. One example could be vesicle adsorption and formation of supported lipid bilayers.
The photobleaching discussed above is not only a drawback in fluorescence microscopy but could be used to study diffusion rates of for example lipids or proteins in SLBs. Fluorescence recovery after photobleaching (FRAP) uses high intensity light (laser) to quickly bleach fluorophores situated in or attached to a SLB, in a well-defined spot. The diffusion of bleached fluorophores out of the area and unbleached ones into the area is then monitored until the time that full recovery of the bleached spot occurs. By looking at the time it takes to recover, the lateral diffusion can be determined[121]. FRAP could, for example, be used to determine lipid or protein diffusion within a SLB or to probe number of multivalent interactions between adsorbed molecules and SLBs (more attachment points gives slower diffusion).[122] Jönsson et al. further improved analysis and availability with a MATLAB script for determining diffusion from FRAP measurements.[44,123]
Fluorescence resonance energy transfer (FRET) is a non-radiative energy transfer between two fluorophores where the emission spectrum of one overlaps the excitation of another fluorophore. When the first type of fluorophore is excited, if there is a second type fluorophore in close enough proximity (~1-10 nm), there will not be any emission from the first, but an energy transfer to the second which then goes on to emit (the transfer is caused by dipole-dipole interactions). This enables studies of interactions between, for example, two proteins, each labeled with one type of fluorophore. Upon excitation of the first type of fluorophore, only the proteins labeled with that fluorophore are visible until proteins with the other type are introduced. Interacting proteins stops emission from fluorophore type A and starts to emit light from fluorophore type B instead.
Some fluorophores are prone to self-quenching at higher concentrations, calcein for example has a concentration regime 6-10 mM where intensity and concentration has a linear relation.[124] This relation could be used in vesicle encapsulated calcein to study changes in fluorescence intensity as an indirect means of probing solute transport across lipid vesicle membranes as changes in vesicle volume. In other cases, carboxyfluorescein is used which has self-quenching properties in response to changes in pH.

4.2 SPR

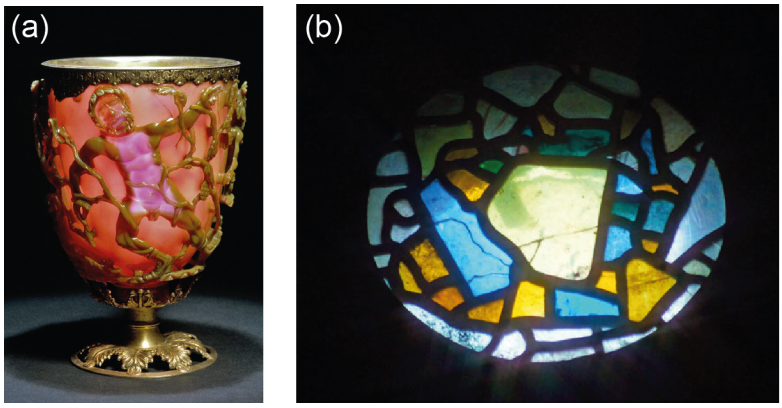

*Fig.26 Early examples of plasmon resonance: (**a**) The lycurgus cup (300 CE). Image from Ref.*[125]*. (**b**) A stained glass window from St. Paul's Monastery in Jarrow, England, founded in 686 AD. Image from Ref.*[126]

Plasmon resonance is a phenomenon that has been observed since even before antiquity in the Lycurgus cup (300 CE) [125] and later in stained glass windows (700 CE), where transmitted light interacts with metal nanoparticles dispersed in the glass in a way so that some of the wavelengths are adsorbed, hence giving the glass an appearance of a color. Surface plasmon resonance was first studied by Wood who observed anomalies in the expected spectrum when shining light on a diffraction grating with metal-backing (compared to without metal-backing)[35,127,128], suggesting that light in some unexpected way interacted with the metal layer. Although attempts were made to understand the phenomenon[129],[130], it was not until 1968 that a full physical explanation could be offered by Kretschmann and Raether[131] and the same year by Otto[132]. They expanded on the theory and discovered ways to use this phenomenon in a setup causing attenuation at a specific angle of the incident light using a prism and a semi-transparent thin metal film. A SPR Kretschmann coupling is shown in **fig.28**. SPR would prove extremely sensitive to changes in refractive index on the side of the thin metal film opposite to the prism. However, it was not until the 1980's, that Liedberg et al. first started to use SPR for biosensing purposes [133], and later the first to develop a commercial instrument, Biacore.

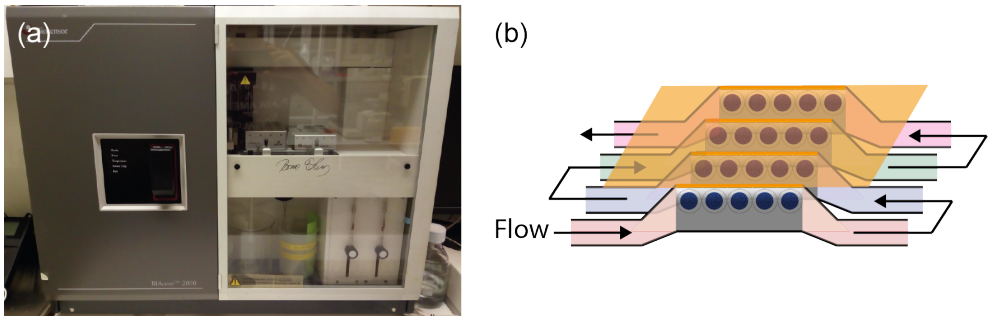

***Fig.27.**(**a**) An SPR instrument, a Biacore 2000, used for the experiments in **paper II**. . It comes with a convenient automated liquid handling system, which allows for very precise injections. It is also programmable so that complex and longer experiments could be done more easily. (**b**) This model has four flow cells which could be used individually or in parallel, which makes it possible to perform different experiments and control experiments simultaneously. This illustration shows serial flow mode, but each channel could also be used separately. In the illustration, chromaffin vesicles are adsorbed to the functionalized Au-surface which sits on top of the flow cell (not to scale). The*

dimensions of the flow cells are very small, surface area A=1.2 mm^2 and the volume of each flow cell is 60 nL.

SPR has an exceptional sensitivity compared to many other techniques and can detect protein binding as low as 1 pg/mm^2 (in **paper II** this limit of detection would correspond to 384 chromaffin vesicles).[134] As a comparison, another widely used technique quartz crystal microbalance (QCM) has a sensitivity of 1 ng/cm^2 (this would correspond to 3.2·10^5 chromaffin vesicles).[135] Some other advantages of SPR is that it is possible to monitor biomolecular interactions in real-time, and also that it, in contrast to for example TIRF-microscopy, is a label-free technique which means that no fluorphores are required to obtain a signal. This is off course a great advantage as there can be no doubts over any possible fluorophore interference. Another benefit of SPR is that it is an ensemble technique, meaning that when looking at for example vesicles you are looking at the average signal from about 10^5 vesicles. This gives extremely sensitive, stable and repeatable measurements. That SPR is an ensemble measurement method, is also a downside as the system cannot observe heterogeneities or sub-populations within any sample. Hence, SPR lends itself best to homogenous samples.

Although there are now many manufacturers of SPR systems, Biacore still remain one of the most sensitive and arguably the most stable and easy to use system. But, other SPR systems can offer new possibilities, as BioNavis which for example produces a dual-wavelength SPR, which makes it possible to obtain the average film thickness of an adsorbed film based on the difference in response for the two wavelengths.[108]

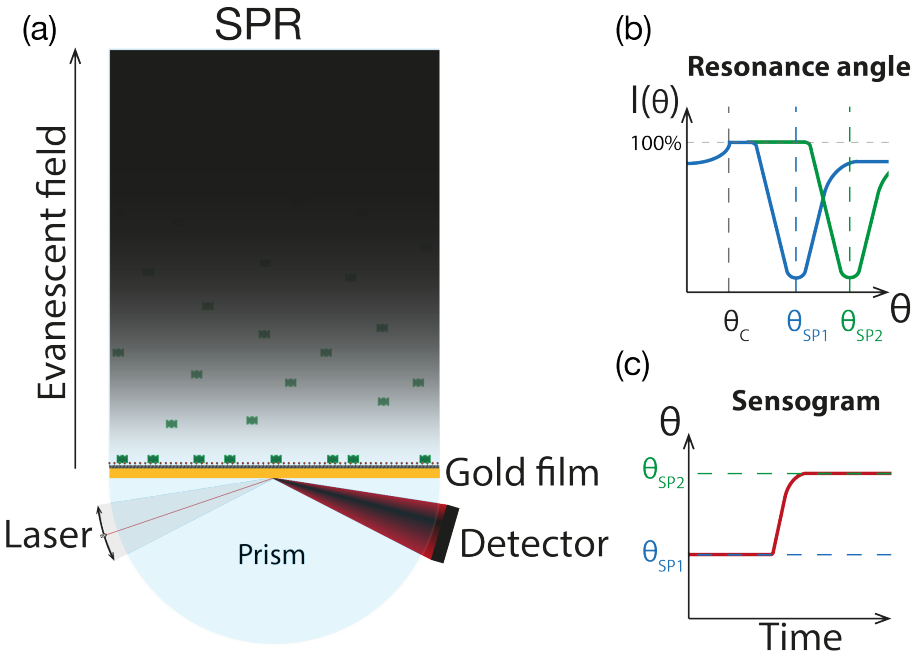

Fig.28.*(**a**) Working principles of the SPR. Light is shone through a prism and reflected against a thin gold film for a span of angles, causing an evanescent wave to form, at a certain angle there is a sharp attenuation in the reflected light due to interaction between the evanescent wave and the molecules in close proximity to the gold film (**b**) As molecules adsorb at the surface, this leads to a change in refractive index which causes the resonance angle ϑ_{SP1} where maximum attenuation happens to change to ϑ_{SP2}. (**c**) The change in angle could be monitored over time in a sensogram*

Surface plasmon resonance is a technique where P-polarized light is scanned over a range of angles above the critical angle θ_C, at and above which total internal reflection occurs, creating an evanescent field, perpendicular to the surface (**fig.28a**). The evanescent waves interact with free electrons in the semi-transparent gold film causing surface plasmon resonance to occur

(collective oscillations of the free electrons in the gold film). The surface plasmon interaction causes attenuation of the reflected light, and at a certain angle θ_{SP1}, corresponding to the refractive index close to the surface, resonance occur giving maximal attenuation of the reflected light (**fig.28b**). The surface resonance is very sensitive and a change in refractive index, from for example molecules adsorbing to the surface, causes a corresponding shift in resonance angle to θ_{SP2} at saturation. The changes in angle at with resonance occur is recorded over time in a sensogram (**fig.28c**). As resonance angle and refractive index are related (see eq. 16), for many instruments the change is often plotted as a response in refractive index units (RIU) or resonance units (RU) for Biacore.

4.2.1 Surface plasmon theory

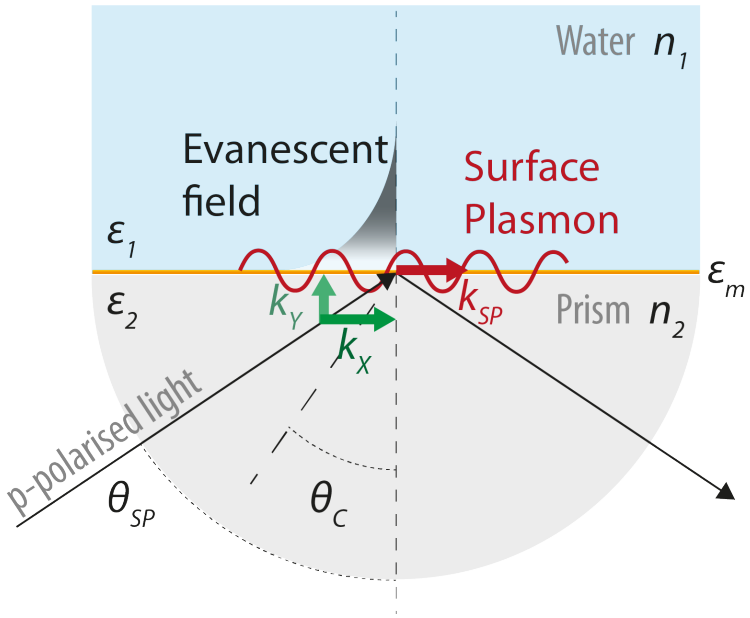

Fig.29. *An illustration of surface plasmon resonance showing the key theoretical concepts. In the illustration k_x is the x-axis component of the incident light wave and k_{sp} is the x-axis component of the plasmonic wave. θ_{SP} is the resonance angle at which surface plasmons occur. ε_1, ε_m and ε_2 are the dielectric constants for water, gold and the prism. n_1 and n_2 are the refractive index of water and the prism.*

The dispersion relation of the incident light could be described as[136]

$$k_x = \frac{\omega}{c}\sqrt{\varepsilon_2}\sin\theta_{SP} \tag{13}$$

, where ω is the angular frequency of the incident light, *c* is the speed of light in vacuum, ε_2 is the dielectric constant of the prism. The dispersion relation of the surface plasmon could be described as

$$k_{SP} = \frac{\omega}{c}\left(\frac{1}{\varepsilon_1}+\frac{1}{\varepsilon_m}\right)^{-1/2} \tag{14}$$

, where ε_1 is the dielectric constant of water ($1.333^2 \approx 1.78$) and $\varepsilon_m(\omega) = \varepsilon'_m(\omega) + i\varepsilon''_m(\omega)$ is the dielectric constant of gold (at λ=760, the real part is $\varepsilon'_m(\omega) = -20.913$ and $i\varepsilon''_m(\omega) \approx 1.2923$, [137], [138] (for a metal the dielectric constant is always negative, $\varepsilon_m < 0$). As $|\varepsilon'_m(\omega)| \gg |\varepsilon''_m(\omega)|$ so we can approximate $\varepsilon_m \approx \varepsilon'_m(\omega)$. Also, with $|\varepsilon_m| \gg |\varepsilon_1|$ we can simplify eq.14 as

$$k_{SP} \approx \frac{\omega}{c}\sqrt{\varepsilon_1} \tag{15}$$

Now, one of the conditions for surface plasmons to occur is that $k_x = k_{sp}$, which gives

$$\sqrt{\varepsilon_2}\sin\theta_{SP} = \sqrt{\varepsilon_1} \quad \Longrightarrow \quad \theta_{SP} = \sin^{-1}\left(\frac{\sqrt{\varepsilon_1}}{\sqrt{\varepsilon_2}}\right) =$$

$$= \left\{n = \sqrt{\varepsilon}\ (non - magnetic\ materials)\right\} \approx \sin^{-1}\left(\frac{n_1}{n_2}\right) \tag{16}$$

, where n_1 is the refractive index of water within the plasmon sensing field and n_2 is the refractive index of the prism. As n_2 is static, θ_{SP} is dependent on refractive index changes within ~150 nm from the surface, which makes it possible to monitor surface based biomolecular interactions. The sensitivity of SPR is very high and could detect changes in refractive index of 10^{-5} units [139] or a shift in the resonance angle of 0.0001° [140], corresponding to roughly a surface protein coverage of 1 pg/mm^2 (CM5 chip) [134].
Eq.16 could be considered a bit surprising, as it turns out to be identical to eq.8 describing the critical angle ϑ_C for TIR. However, by contrast, in this system there is a 50 nm thin gold film in between the prism and the water, which means that the critical angle ϑ_C for this system rather is given by

$$\theta_C = \sin^{-1}\left(\frac{n_{gold}(\lambda)}{n_2}\right) = \left\{n_{gold}(760\ nm) = 0.14123\right\} \approx 5.4° \tag{17}$$

Also, eq. 16 is a simplification showing how the resonance angle θ_{SP} is dependent on the refractive index n_1 close to the sensor surface. Without the simplification introduced in eq.11, θ_{SP}≈68.4°, by contrast the simplification in eq.16 gives θ_{SP}≈66.5° (with n_2 = 1.45).
Signal response ΔR for a thin adsorbed film of a solute is given by

$$\Delta R = S(\Delta n)e^{-(2d_{eff}/\delta)} \tag{18}$$

, where S is a sensitivity constant (1*10^6 for Biacore), Δn=(n_{solute} - n_{bulk}) is the difference between the refractive index of the bulk solution and of the solute. All is scaled with the intensity for the film at the given effective film thickness d_{eff} where δ is the decay length of the sensing field (≈ 150 nm for Biacore) [141].
For studying vesicle adsorption, we can use an expansion of eq.18 in a form applicable to vesicles instead of thin films [108]

$$R = S(n_{vesicle} - n_{bulk}) * c_c * V_v * (1 - \mathrm{e}^{-\frac{2\mathrm{r}}{\delta}})/2\mathrm{r} \tag{19}$$

, where S is the sensitivity of the Biacore instrument used, $n_{vesicle}$ and n_{bulk} is the refractive index of the lipid membrane and of the bulk solution, c_c is the surface coverage of vesicles (#/mm^2), V_v is the membrane volume of one vesicle, r is the vesicle outer radius and δ is the decay length of the evanescent field. From this we can obtain the surface concentration of vesicles, which is a useful information.

Further, the mass per area of an adsorbed film could be expressed as

$$\Delta\Gamma = \frac{(n_{eff} - n_{bulk}) * d_{eff}}{dn/dC} = \{Applying\ eq.\ 18\} =$$

$$= \frac{d_{eff}}{S(dn/dC)e^{-(2d_{eff}/\delta)}} \Delta RU \quad (20)$$

, where n_{eff} is the effective refractive index of the absorbed film, d_{eff} the effective thickness of the adsorbed film, *dn/dC* is the change in bulk refractive index per solute concentration increase, S is the sensitivity of the instrument (10^6) and δ is the sensing depth of the evanescent field.[141,142]

4.2.2 Applications

The most common application for SPR is to study binding and release kinetics to determine the affinity of some binding reaction. This could for example be used to determine how effective a drug candidate is towards a specific target by looking at the affinity, the higher the affinity, the better the candidate is at blocking the drug target.
In **paper II** we use SPR to measure passive transport across lipid membranes of surface attached lipid vesicles, as first done by.[110] We further use bulk shifts, switching between buffer with ordinary and heavy water, to determine the hydration level of the dense protein core of chromaffin vesicles.

4.2.3 Experimental considerations

Different surface modifications could be employed. For many binding affinity studies a chip with a dextran-matrix is often used, a ligand is then covalently bound to the matrix, after which some analyte is introduced. The covalent bond means that there is no release of the ligand, and the only kinetics monitored is that of the analyte (the ligand could for example be an antibody and the analyte an antigen). The dextran matrix is about 100 nm thick.
For our purposes, looking at surface attached vesicles, we need a thinner coupling chemistry to get the vesicles into the field of view. Frequently we use HS-PEG/HS-PEGBiotin in a 99:1 ratio, the PEG is short 1.5/2.5 nm, which gives a coupling very close to the surface. The downside to this approach is that on longer timescales perhaps 1/10th of the NeutrAvidin tends to come off, so optimally one should remove this release from the acquired data especially for measurements over long timescales. A way to circumvent this potential problem is to use 16-mercaptoundocanoic acid to which NeutrAvidin(NA) or Streptavidin(SA) could be covalently bound via EDC-,NHS coupling chemistry. The covalent bond hinders NA and SA to come off. The drawback is that the EDC-,NHS chemicals degrade over time(months), so that one needs to have fresh batches around.
The biggest problem in longer SPR measurements is air bubbles which could remove parts of most of things not bound hard enough to the surface. For this reason, it is important to both filter, but more importantly to degas the running buffer thoroughly.

4.3 Amperometry

A carbon fiber electrode is dipped into a vesicle solution to probe electroactive cargo of carrier lipid vesicles. As a voltage is applied with the electrode used as either anode or cathode, depending on the electrochemical nature of the molecules to be studied, vesicles coming into close enough proximity to the electrode burst and the electroactive molecules are released and

either oxidized at the sensor surface when used as an anode or reduced when used as a cathode. The oxidation or reduction results in spikes in the applied current. The total amplitudes of the spikes of a bursting vesicle event could be converted to the total number of oxidized molecules.[143]
In our case in **paper II**, we studied the release of catecholamines from chromaffin vesicles. Amperometry could be carried out as either single-potential amperometry or pulsed amperometry, the latter used for electroactive molecules that tend to foul the sensor surface (thereby reducing signal strength).[144] Our measurements were performed with single potential amperometry. Amperometry measurements were carried out in order to compare the release in amperometry to the one seen in SPR measurements (for LDCVs having undergone similar treatments).

4.4 Determining vesicle size

For nearly all studies involving lipids vesicles it is crucial to know the size of the vesicles. Whether it is to relate vesicle volume, curvature, surface area to permeability, number of proteins, linkers, fluorophores per vesicle, loading volumes, protein functionality vs. curvature etc.
The techniques used to determine vesicle sizes can be divided into two groups: techniques that measure dry or hydrodynamic size. Dry size is the actual physical size of the lipid vesicles whereas hydrodynamical size is the size of the lipid vesicle with added hydration shells (vesicles in solution makes the water molecules closest to it order themselves and move with the vesicle, thus contributing to the measured size). The most common dry size methods are cryo-TEM[145] and freeze-fracture SEM.[146] The hydrodynamical measurement techniques as NTA and DLS are the most commonly used as they are very fast, inexpensive and easy to use in comparison.

4.4.1 NTA

NTA is preferred when working with polydisperse vesicle size distributions as it monitors and estimates the size of each particle separately without large particles dominating the signal. It accurately measure the hydrodynamic size of particles and tend to give slightly smaller size estimates in comparison with DLS.[147]
In NTA a laser beam is progressing through a prism and any particles it encounters way will cause light to scatter, it is this scattered light with focus in the focal plane which is caught by an objective and recorded with a CCD-camera. The recording is a 2D representation of the particles free to diffuse around in 3D in the bulk. Fortunately, it is enough to follow the particle diffusion in 2D to determine its size. The software records all diffusion tracks from the particles. The recorded tracks for each particle is then used in single particle tracking (SPT), where the mean square displacement (MSD), as an average from all time intervals, is determined and translated into diffusivity. The diffusivity of each particle is then converted to size using the Stokes-Einstein relation (see eq.1).[148] Using NTA it is important not to have too many particles in the solution(~100 particles per frame is optimal) as the particles then are more probable to cross over each other in bulk and the system first following one particle may continue to follow the other and so the determined size is a mixture of the two. For results to be more optimal it is important to increase statistics by following as many vesicles as possible for as long as possible. This could be achieved by making long enough recordings and to record at least five times, injecting new particles before every measurement to ensure that not the same particles are measured again, or to use a syringe pump with a constant flow during the measurements. However, using a syringe pump always tend to give slightly smaller estimates of particle sizes

(from experimental experience). Also, it is easy to end up with slightly different results depending on parameter setting in the software, so for comparative studies these should preferably always be set in the same way. Using the Stokes-Einstein relation we notice the importance om monitoring the temperature or to fixate it and using the correct viscosity of the particle solution. Each particle is surrounded by a static film of water molecules, created by a dipole moment induced by the particle charge. This static film adds to the particle size observed, and thus we measure the hydrodynamic size of the particle.

4.4.2 DLS

Dynamic light scattering (DLS) is preferably used with monodisperse vesicle size distributions as it works with fluctuations in total scattering intensity and larger particles scatters more, and hence its fluctuations for the larger particles that dominates the signal. DLS uses a laser beam and shines it through a cuvette with a particle solution. As the light interacts with the particles it scatters homogenously in all directions. The total scattered light for all detected particles is now followed over time. What is seen is that the total intensity fluctuates over time due to changing constructive/destructive interference between the scattered light from the particles. These fluctuations are then looked at in an autocorrelation function where particles diffusing at different rates show different decay times for increasing time intervals.[149] The autocorrelation function can then be related to the diffusivity. From diffusivity the Stokes-Einstein relation (see eq.1) is then used to determine particle size. Also, here, using the Stokes-Einstein relation, we understand that it is important to monitor the temperature and use the correct viscosity. In solution a particles charge creates a dipole moment and the water molecules closest to the particle creates a film, static ordered water molecules also affects the scattering, so in this way, using DLS, one gets the hydrodynamic size of the particles.

4.4.3 TEM

Transmission electron microscopy (TEM) uses high vacuum which tends to deform soft particles like lipid vesicles, but for the images used in **paper II** (**fig.4**), vesicles were first fixated chemically (Karnovsky fixative). An electron beam is transmitted through the thin sample and collected. The intensity of transmitted electrons in each point depends on the density of the sample, in this way a high resolution image is possible to obtain.

5 Summary of papers

5.1 Paper I - Total internal reflection fluorescence microscopy for determination of size of individual immobilized vesicles: Theory and experiment

It was found that the theoretical expressions derived and used in many papers for correlating vesicle size with the intensity of membrane embedded fluoresecnt dyes were incorrect. For smaller vesicles, this did not present significant error, but for larger ones their converted sizes were found to be grossly exaggerated (Fig.26).

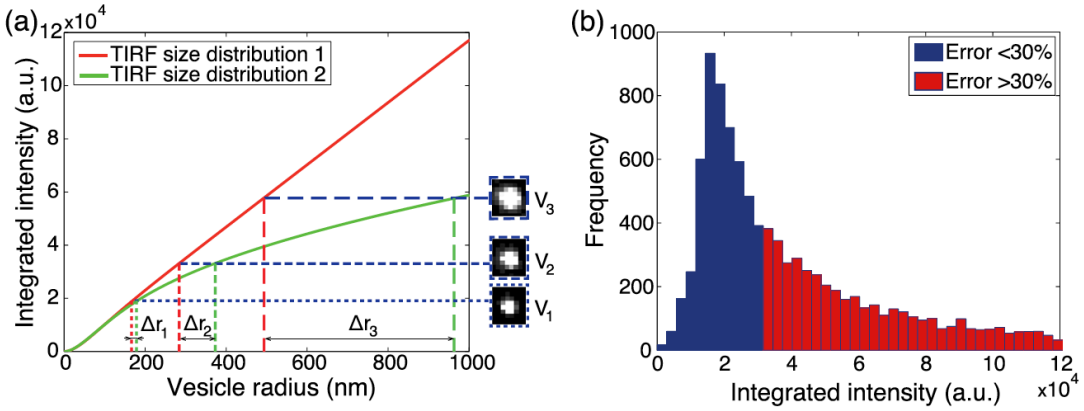

Fig.30. *(**a**) Intensity to radius using eq. 21 (red) and the erratic eq. 24 (green) using δ = 100 nm. There are three micrographs (1.6x1.8 μm²), portraying three vesicles of different sizes. For the smallest vesicle the difference in size estimate is negligible, but for the largest one the erratic eq. 24 converts the intensity to a size twice the one obtained from eq. 21. (**b**) Shows the frequency of recorded vesicles of different integrated intensities, using eq. 21 and eq. 24 it is shown above which integrated intensities that there is a discrepancy in the size conversions smaller than 30% (in blue), and larger than 30% (in red).*

The problem with eq.24 (see below) used in many papers, is that cylindrical vesicle membrane segments were integrated to determine the surface area of a sphere. The equations suggested, using polar coordinates instead of Cartesian, adds instead of cylindrical segments, segments with the correct curvature to integrate the surface area of a sphere.
150

Result of our formalism using spherical coordinates:

$$I(r) = 2\pi A J_0 r\delta[1 - \exp(-2r/\delta)], \quad \text{or} \tag{21}$$

$$I(r) = 4\pi A J_0 r^2 \quad \text{at} \quad r \ll \delta, \quad \text{and} \tag{22}$$

$$I(r) = 2\pi A J_0 r\delta \quad \text{at} \quad r \gg \delta \tag{23}$$

Where J_0 is the intensity of the incident light and *A* is a constant proportional to the dye concentration and absorption cross section.
Result of previous erratic formalism using cartesian coordinates

$$I(r) = 2\pi A J_0 \int_0^{2r} (2rz - z^2)^{1/2} \exp(-z/\delta) dz, \quad \text{or} \tag{24}$$

$$I(r) = 2\pi A J_0 r^2 \quad \text{at} \quad r \ll \delta, \quad \text{and} \tag{25}$$

$$I(r) = 2^{1/2}\pi^{3/2} A J_0 r^{1/2}\delta^{3/2} \quad \text{at} \quad r \gg \delta. \tag{26}$$

We notice that for small vesicles (where $r \ll \delta$) eq.22 and eq.25 are similar (by using different A's). However, for large vesicles (where $r \gg \delta$), we see that the intensity *I(r)* in eq.23 is proportional to *r*, while in the corresponding eq.26 the intensity *I(r)* is proportional to $r^{1/2}$, this obviously results in a large discrepancy between size estimates for large sized vesicles (**fig.30a,b**).

To experimentally investigate this potential error, we used recordings of > 10000 individual vesicles observed in TIRF microscopy and analyzed the total intensity of each vesicle using a MATLAB script that identifies all the pixels belonging to each vesicle and sums them up to a total intensity (after subtracting the background intensity). The fluorescence intensity is proportional, in accordance with eq.21, to the vesicle size and the distribution in intensity corresponds to the distribution in vesicle size. The size distribution of the vesicle sample was measured in nanoparticle tracking analysis (NTA) in suspension (>10000 tracks were collected), the immobilized vesicles on the other hand is affected by diffusion and since the smaller vesicles diffuse faster, the size distribution seen in NTA gets a corresponding distribution on the surface skewed towards smaller vesicle size according to a formula we present. We made a MATLAB script to convert the size distribution from NTA to the corresponding size distribution of immobilized vesicles using:

$$\mathcal{F}(r) = r^{-\beta}F(r) / \int_{r_{\min}}^{r_{\max}} r^{-\beta}F(r)dr, \tag{27}$$

where r_{min} and r_{max} are the minimum and maximum vesicle radii. For cases with low or no flow β = 1/2 and for high flow β = 2/3.

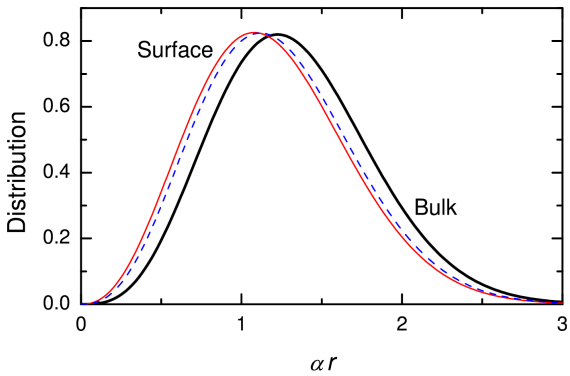

Fig. 31. *Size distribution in bulk solution (black) and the two corresponding size distributions of vesicles immobilized on a surface. The surface distributions were calculated using eq.27 with β = 1/2 (dashed blue) and 2/3 (red).*

Comparing two distributions, as we do here between intensity distribution and size distributions from NTA (**fig32.a,b**), it is of course critical to use the same number of bins for the sizes converted from the total intensity distribution as used in the NTA results (default bin size width in NTA is 0.5 nm). It is however not unusual to see papers where two distributions are compared which are binned differently, this is obviously not correct as the shape of a distribution will change depending on how many bins the data is divided into (amplitude, broadness of peaks, amplification or suppression of features in the curve).

We then correlated the size distribution on the surface with the size distribution obtained from the total intensity distribution of the vesicles using eq.21, in order to extract the constant $B = AJ_0$ needed for conversion between total intensity and size. The constant was obtained as the value that makes the centroids of the peaks of the two distributions intersect. This calibration should preferably be done for each measurement (i.e. calibrate the intensity to size distribution). We made a MATLAB script that takes the two distributions and correlates them by finding the optimal value of *B*. Eq.21 could then be used to convert the total intensity of any vesicle to corresponding size.

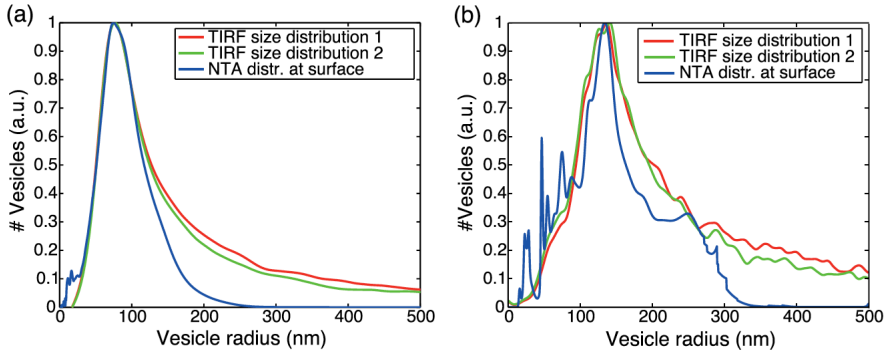

Fig.32. *(**a**) TIRFM size distributions of monodisperse lipid vesicles obtained by converting integrated intensity of each vesicle to size using eq.21 (red) and the erratic eq.24 (green) using δ = 100 nm. (**b**) same as (a) but for polydisperse vesicle sample. Also shown in (**a**) and (**b**) is the NTA vesicle size distribution (diffusion corrected)*

In **fig.32a,b** one can see that for both vesicle distributions, while the size distributions agree rather well to the left hand side of the main peak of each distribution, on the right hand side there are tails for the distributions converted from total vesicle intensities. This could mean that some vesicles although precaution was taken, may have been flattened towards the surface, placing more of the vesicle fluorophores within the evanescent field. But, as the tail continues far to the right, a more probable explanation is that although the vesicles were freeze-thawed and extruded, a fraction of them had multiple lipid bilayer shells (MLVs). It has been shown that extrusion through membranes with large sized pores (as used in the paper) are not as effective at reducing multilamellarity as membranes with smaller pore sizes.[151]
So, some caution should still be employed when drawing conclusions from larger sized vesicles, hopefully, as the multilaminar vesicles are fewer, this may show up as a discrepancy in some measured function and those results could be removed (for example, the protein function of a small fraction of the larger vesicles may be similar to that of the smaller sized ones and could therefore be regarded as MLVs with some caution).

5.2 Paper II - Content and Dense-Core Quantification of Chromaffin Vesicles using Surface Plasmon Resonance

In this paper we used surface plasmon resonance to study isolated chromaffin vesicles immobilized on a SPR sensor surface(**fig.19**), with the aim to study release of stored cathecolamines (dopamine, adrenaline, nor-adrenaline) stimulated by hyperosmotic stress (**fig.33**). In this way we intended to verify an earlier study that showed a decrease in catecholamine content for intracellular chromaffin vesicles when the hosting cells were subjected a hyperosmotic shock.[152] This way, one should be able to assert that the vesicles had not lost their initial cathecholamine loading (~0.35-1 M)[152–155] during isolation, purification and immobilizion steps. In addition, such measurements should enable a comparison of the release

observed in amperometry with the releaseobserved using SPR, as well as to be able to study the catecholamine release kinetics. A hope was also to be able to discern a possible difference in release rates between release from catecholamines bound to ATP in the vesicle halo, compared to release of catecholamines bound to the dense protein matrix. As could be seen in **fig.33a** for chromaffin vesicles (in blue), we discern multiple release reactions; the first one is a very fast (< 0.1 s) and displays a magnitude of ~78 RU (**fig. 33b**), appearing when the buffer is switched from being H_20-based to being based on D_2O (heavy water). The pH of D_20 is about 0.4 higher than for H_2O, and as the aggregates of three catechols to one ATP is electrostatically bound,[156,157] a change in pH may change the strength of the association. Curiously it is when swiching back again from D_2O to H_2O that the rapid release occurs, which was discerned by comparing the amplitude of the D_2O shift from right and from left with the amplitude of subsequent D_2O-switches. The second release ~250 RU is also very rapid (< 0.1s) and occur as a 400 mM Sucrose hyperosmotic shock is applied. This fast release in SPR corresponds to 0.58 million released catecholamines in comparison to 1.4 million as reported in Ref.[152]. Our SPR data suggested a total catecholamine concentration in the vesicles of 0.38 M (assuming all catecholamines were released). However, the amperometry meausurement suggested a 1.49 M catecholamine loading for vesicle batches prepared in a similar fashion to those used in SPR. The drop seen in in amperometry of catecholamine loading was about 37% between LDCVs in isoosmolar buffer and hyperosmotic buffer, while in SPR the fast 250 RU release seen at the initiation of the hyperosmotic sucrose shock corresponds to ~40% of the total release in SPR (**fig.33b**). Actually, there is nothing to suggest that we would be able to achieve complete release of all stored catecholamines only by employing osmotic shocks, as it does not mimic how release is controlled in the body, nor in amperometric measurements.[10] In the chromaffin cells, the vesicles fuse with the membrane either completely or partially, to achieve total release, which means that they expose their intravesicular environment with pH 5.5 to the extracellular solution with pH 7.4. In the amperometric measurements the vesicles encounter an electrode and burst, the electroactive species in the vesicles oxidizes at the electrode surface (catecholamines donates two electrons at oxidation), this creates a signal giving the total number of electrons given by each vesicle bursting event. This means that the whole content of the vesicles is emptied during the amperometric measurements and may offer an explanation to the difference in total catecholamine concentration for the vesicles reached by SPR and amperometry. Also, in amperometry all electroactive species are recorded as the oxidise, ADP gives off one electron if it oxidises and AMP probably two. Their concentrations are however rather low compared to the catecholamines and would probably not affect the catecholamine concentration estimate significantly. But still, it is possible that some parts of the signal attributed to catecholamine oxidation may stem from other electroactive species present.

Returning to **figure 33**, that is the SPR data and the sucrose injection, one can see that although there is a fast release at the start of the osmotic shock, but for the rest of the duration of the applied osmotic shock however, there is no release observed as the profile of the curve is identical to the ones of subsequent sucrose injections (subsequent sucrose injections show no release, profile comparison not shown). However, as the sucrose injection finishes and the flow return to only buffer, another release is observed where it is possible to resolve the kinetics (**fig.33c**). In this release, there is a slow release ~90 RU (red dotted line), and a ten times faster one ~90 RU. Our hypothesis is that the fast release kinetics seen may refer to cathecholamine release from the halo, and the slower one catecholamine release from the dense protein matrix (where it is bound with higher affinity). However, as catechols are released from the halo (and possibly dense core), the nucleotides ATP, ADP and AMP may be released as well. If so, the catecholamines and nucleotides are expected to have different permeability through the membrane. For this reason, it is at this point not fully clear what the two kinetic regimes refer to. During a subsequent loading of 400 mM xylitol, we also see that there is a release going on at the

same time as the xylitol is loaded into the vesicles (could be seen by comparing the profile during loading for blue and red curves).

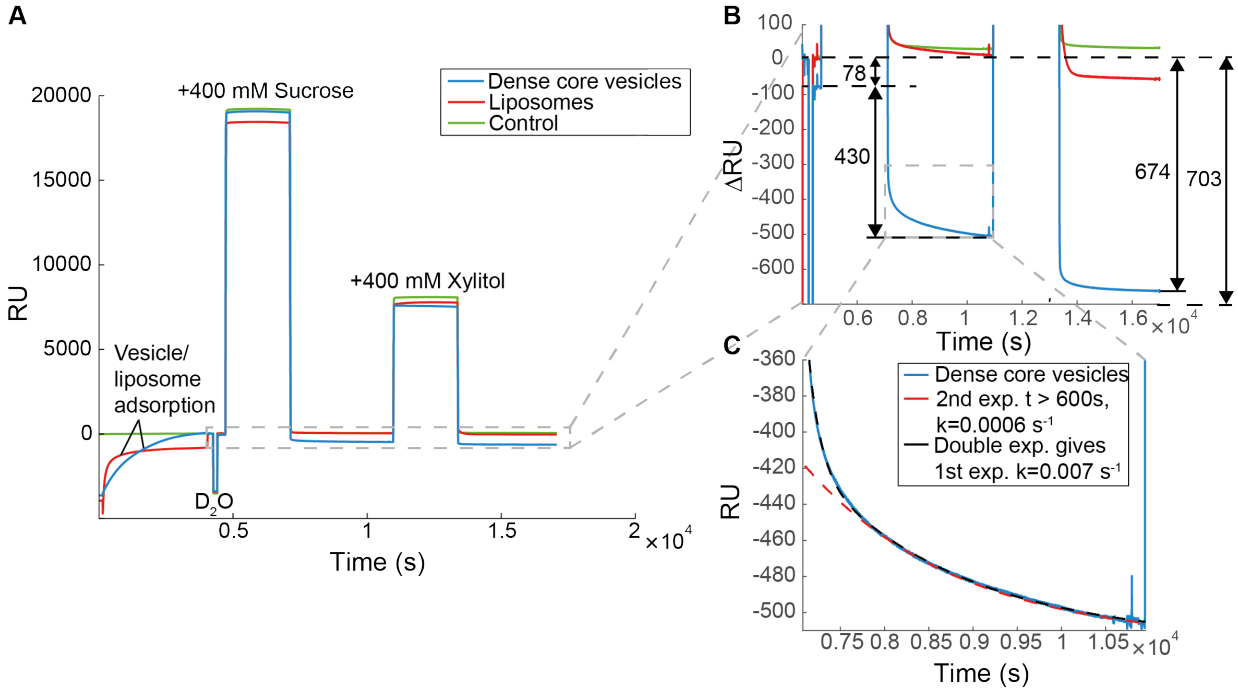

Fig.33.*(**a**) Starting at t=0 s, the left graph shows the signal response upon adsorption of LDCVs in isotonic conditions (310 mOsm/kg) in one channel (blue), liposomes in another (red), as well as for a channel without vesicles/liposomes (green). This was followed by simultaneous incubations in all three channels of i) D_2O buffers for 100 s, ii) 400 mM sucrose (710 mOsm/kg) for 2000 s and 400 mM xylitol (710 mOsm/kg) for 2000 s. (**b**) shows a magnification of the signal response when switching back to running buffer subsequently to the sucrose and xylitol incubations. (**c**) shows a magnification of the slow phase after interruption of the sucrose incubation.*

We also use a new technique to quantify the number of immobilized chromaffin vesicles on the sensor surface as well as to look at how much of the protein dense core volume is solids. This was done by exchanging the running buffer for a corresponding buffer with D_2O instead, with estimates of the refractive index of the proteins in the dense core and membrane, as well as estimates from of the membrane volume, we can solve for the dense core molecular volume. An added assumption that we make is also that the vesicle halo after release have a refractive index close to that of the outside buffer.

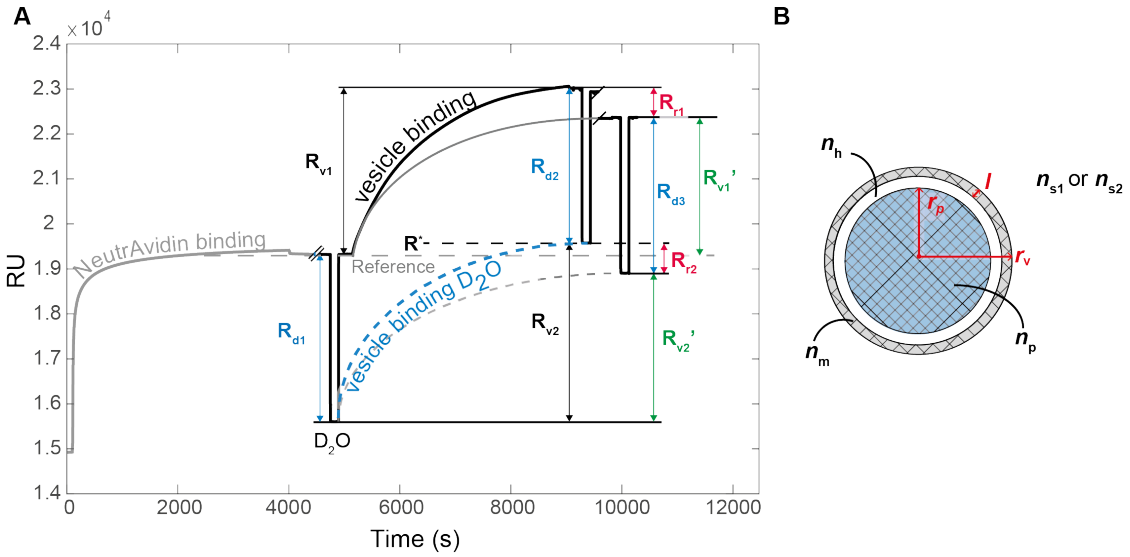

Figure 34: *(**a**): The response upon LDCV binding, R_{v1} = 3690 RU, to a NeutrAvidin modified surface, including buffer exchange from H_2O to D_2O buffers before, R_{d1} = 3716 RU, and after, R_{d2} = 3442 RU, vesicle adsorption. Also shown are the magnitudes of osmotic induced content release, R_{r1} = 704 RU, (see figure 4 for details), and subsequent exchange form H_2O to D_2O buffers, R_{d3} = 3462 RU. The dashed lines depict the corresponding vesicle binding in buffer with D_2O before, R_{v1}' = 3070 RU, and after, R_{v2}' = 3199 RU. (**b**) Illustration of refractive index distributions of the LDCV vesicles with radius r_v. An outer membrane with thickness l and refractive index n_m. A solute halo with refractive index n_h. Dense core with radius r_p and effective refractive index n_p.*

$$R'_{v1} = Sc_v[(n_m - n_{s1})V_m + (n_p - n_{s1})V_p]\delta^{-1}\varphi(r/\delta) \quad (28)$$

$$R'_{v2} = Sc_v[(n_m - n_{s2})V_m + (n_p - n_{s2})V_p]\delta^{-1}\varphi(r/\delta) \quad (29)$$

where R_{v1}' and R_{v2}' correspond to the SPR response for vesicles in H_2O and D_2O after content release, respectively (**Fig.34a**). By taking the ratio of Eqs. (28) and (29), and with n_{s1}=1.33 and n_{s2}=1.3246 (at λ=760 nm),[158,159] one finds that the remaining unknown parameters are reduced to n_m, n_p , V_m, and V_p. Further, using R'_{v1} = 3070 RU and R'_{v2} = 3344 RU, and by assuming a membrane thickness *l* of 6.5 nm,[155] and a membrane refractive index, n_m, of ~1.5 (i.e. ~51% phospholipids, 16% cholesterol and ~33% proteins[160], with respective refractive indices of $n_{phospholipid} = 1.48$ (Ref.[161]), $n_{cholesterol} = 1.525$ (Ref.[162]) and $n_p = 1.52$ (Ref.[163]), one can estimate the molecular volume of the dense core comparable to that of a sphere with r_p ~65 nm.

In combination with size measurements of the dense core in TEM (**fig.4**), we could then estimate the hydration level of the dense core to **65%**. Although the dense protein matrix looks solid in the when negatively stained in the TEM images, it is rather like a spongelike structure. With our method we estimate how much of that sponge is solid.

Comparing our values with values from literature

Estimate1:

The composition of the chromaffin vesicle is described in detail in Ref.[157], which makes it possible for us to use these values to make an estimate to use as a comparison with our experimentally derived values. For the membrane content are listed the following components: Dopamine β-hydroxylase Mw=280000 g/mol, Cytochrome b-561 Mw=21000 g/mol, ATPase Mw=400000 g/mol, Phospholipids Mw ≈ 750 g/mol (used in [157]) and cholesterol Mw=386.65 g/mol.[162]. The dense protein matrix consists to the largest part of the protein Chromogranin A with Mw ≈ 74.000-81.200 g/mol,[164] Dopamine β-hydroxylase, *Leucine enkephalin* Mw 555.632 g/mol [165] (minor part Met-enkephalin Mw 573.226 g/mol [166])

Taking the total protein weight of the dense core (from Dopamine β-hydroxylase, Chromogranin A and Met- and leu-enkephalin, table 3) and dividing it with a protein density 1.4 g/cm^3 gives a radius of the dense core of **50 nm**.

Now, 35% of the ATP is suggested to be bound to the Chromogranin A proteins in the dense core [157]. The number of ATP molecules in the soluble content would correspond to $4900 \cdot (5000/36)$ using conversion relations between table 2 and 3 in ref.[157], hence if 35% of these are bound to the dense core we would get an additional volume of $((0.35 \cdot 4900 \cdot (5000/36))/(6.022 \cdot 10^{23})) \cdot 192.4 \approx 7.61 \cdot 10^{-17}$ cm^3 (Molar Volume ATP: 192.4±7.0 cm^3) [167]. If this volume is added, then the radius of the dense core becomes **52 nm**

Note that this estimate does not represent the hydrodynamic volume, but neither does the estimate from the H_2O:D_2O method. Further, in this estimate only ATP was assumed to bind to the dense core as well as forming aggregates with catecholamines, ATP makes up ~71% of the nucleotide total. We did not consider the other nucleotides that also forms aggregates with catecholamines, as these represent only a minor part of the nucleotides in the chromaffin vesicles and as they bind catecholamines at lower ratios (ADP binds catecholamines at a 1:2 ratio and AMP at a 1:1 ratio) [157].

Dense core bound catecholamines add significant volume to the dense protein core size estimate

If the number of dense core bound ATPis 35%, as stated above, then the number of free ATP in the halo is $(0.65 \cdot 4900 \cdot (5000/36)) \approx 440000$ (converting values from table 2 to corresponding table 3 values in ref.[157]), of which each bind in aggregates with three catecholamines,[157] this means that the number bound to the dense core could be as much as 3000000-1320000 = 1680000. If unreleased, this would in turn give an added volume to the dense core of $(1680000/(6.022 \cdot 10^{23})) \cdot 142.7 \approx 3.98 \cdot 10^{-16}$ cm^3 (Adrenaline molar volume 142.7 cm^3/mol [168]). Together with 35% of the ATP bound to the dense core this would give a dense core radius of about **63 nm**.

Looking at our release as seen in SPR and comparing the number of catecholamines still bound to the dense core, and what size the dense core would have

If the total of the initial loading is $3 \cdot 10^6$ as suggested in ref.[157], and the total release that we observed in SPR was $1.22 \cdot 10^6$ catecholamines, then potentially $1.78 \cdot 10^6$ catecholamines remain. This would be more than the ones initially bound to the dense core. Hence, the release seen

could instead be from the aggregates in the halo (as the catecholamines are suggested to bind harder to the dense core). For us this would mean that with the catecholamines initially bound to the dense core still there after release, the possible decrease in dense core volume from released catecholamines would not happen. Thus, the experimentally derived estimate from our H_2O:D_2O-method of a dense core radius of **65 nm**, under the assumption of no release from the dense core, correspond rather well to the values calculated from literature in this estimate. With only the proteins in the dense core, the volume of the dense core would correspond to a **50 nm** radius sphere, a dense core with ATP to a radius of **52 nm** and a dense core with bound catecholamines to a radius of **63 nm**. This would mean that the hydration level ranges between **67.9%** for the fully loaded dense core and **84.0%** for the empty one. The corresponding hydration level for the dense core volume estimate from the H2O:D2O-method comes to **65%**. Generally though, for all hydration estimates of the dense core, it is however not clear if the vesicles imaged in TEM have fully loaded dense cores, empty or in between, and whether this would affect the apparent dense core size seen in TEM.

Estimate 2:

It is also worth noting that previous studies suggest that *the membrane* of the LDCVs contain volume fractions of $v_{\text{protein membr.}} = 0.33$, $v_{\text{phospholipid membr.}} = 0.51$ and $v_{\text{cholesterol membr.}} = 0.16$,[160,164] and a *total protein volume fraction(for both membrane and dense core)* of the LDCVs of $v_{\text{protein LDCV}} = 0.606$ (converted from weight% from Winkler et al. 1976, table 2,[164] using a protein density of 1.4 g/cm^3,[169] excluding catecholamines and nucleotides). This means that the total lipid volume fraction of the whole LDCV is $v_{\text{lipid LDCV}} = 1 - v_{\text{protein LDCV}} = 0.394$, while for only the membrane it is $v_{\text{phospholipid membr.}} + v_{\text{cholesterol membr}} = 0.67$. Now it is possible to express the unknown volume of the dense core V_p in terms of the membrane volume V_m that we have an estimate for. We can do this by comparing the volume fraction of lipids for both membrane and dense core, which is equal to the volume fraction of lipids in the membrane (as lipids are only present there):

$$v_{\text{lipid LDCV}} \cdot (V_{\text{m}} + V_{\text{p}}) = v_{\text{lipid membr.}} \cdot V_{\text{m}} \tag{30}$$

Solving for V_{p} gives

$$V_{\text{p}} = ((v_{\text{lipid membr.}} - v_{\text{lipid LDCV}}) \cdot V_{\text{m}})/v_{\text{lipid LDCV}} \tag{31}$$

This means that $V_{\text{p}} = 0.7V_m$, and r_{p} of 61 nm which gives a hydration level of 71%, which is close to the values obtained from the D_2O:H_2O method used in the article.

Estimate 3:

Also, Morris et al.[38] estimates the volume fraction of the solid part of the solute depleted dense protein core to 0.375 times the LDCV volume, which instead gives a radius r_{p} of 92.3 nm for a *hydrated* dense core depleted of catecholamines, and could be compared to the size determined from TEM of 92 nm (which shows the hydrated dense core).

	r_p (nm)		*Hydration level of dense core (%)*
H_2O:D_2O-method	65	*(~Loaded)*	65
Estimate 1	50-63	*(Empty-Loaded)*	84-67.9
Estimate 2	61	*(Empty)*	71

Estimate 3	92.3	100
TEM	92	100

Table 1. Summary of estimates of dense core solid volume as a solid sphere with radius r_p. Estimated dense core sizes were calculated from references as described in the text.

In table 1 we see that our estimate from the D_2O:H_2O-method corresponds rather well with values calculated from literature. Interesting to see is that the calculations for the first estimate, which gives a span of dense core sizes depending on if it is fully loaded with ATP and catecholamines or depleted. The third estimate of a hydrated volume also corresponds rather well with the size determinations of the dense core from TEM. However, the estimates are based on simplifications and assumptions and should therefore be used with caution.

6 Outlook

In **paper I**, we provided corrections to previous derivations, making it possible to study properties for larger vesicles in microscopy with higher accuracy. Revisiting previous publications for larger sizes of vesicles with the discrepancy in mind could help to better understand experimental outcomes and conclusions. Hopefully, the field will pick up on the corrected formalism. The main challenge for experiments correlating vesicle properties to vesicle size now lies in obtaining more unilamellar vesicles, also for larger sized ones. One scheme for increasing the ratio of unilamellar vs. multilamellar vesicles, could be to include a centrifugation step, optimized so that the heavier multilamellar vesicles start to pellet (without pelleting the large sized unilamellar vesicles), and then use the vesicles in the supernatant for experiments. One may also strive for size determination of immobilized vesicles that does not rely on the content of fluorescent dyes, as recently presented[94]which should help correlating vesicle size to molecular content.

Paper II introduces SPR as a new platform to study chromaffin vesicles. Upon immobilization of chromaffin vesicles on an inert surface one could study transport kinetics across the membrane. As the chromaffin vesicles after all preparation steps were found to maintain their initial loading of catecholamines (as shown by amperometry), one can envision studies in which pore formation in the vesicle membrane is deliberately induced, thereby mimicking exocytosis, where the inner pH of 5.5 would be brought up to 7.4 by the surrounding buffer, or perhaps simulatenously switched for a buffer that is not isoosmolar but reflects the extracellular chemical conditions. Bringing up the pH to 7.4 has been suggested as a release stimuli as the . An alternative to induced poreformation is to shift pH by adding for example NH_4, which easily passes through the membranes of the immobilized vesicles,[170] thereby raising the pH. Pore formation could prove disadvantageous in SPR as it is thought that also short peptides are released from the dense protein core during exocytosis, and SPR would not be able to discriminate between such a release and the release of catecholamines. In a combined approach however, if total release could be induced by an increase in pH (peptides are unlikely to pass through the membrane), then a second step with pore formation would perhaps only show the peptide release.
Another interesting extension of paper II would be to study the reloading mechanisms by putting the vesicles in 2 mM dopamine concentration, as present in the cytosol of chromaffin cells, and adding ATP to the solution. ATP addition after induced release could activate the membrane proteins in the vesicles to reset the pH to 5.5 (V-ATPase) and to actively shuttle dopamine across by a transporter protein (VMAT) in the membrane of the vesicles.
The possible studies are indeed many, as immobilized vesicles allow for repeated experiments on the same set of vesicles, offers very high sensitivity in SPR and the option to switch surrounding solutes at will.

7 Acknowledgements

I want to thank my main supervisor Fredrik Höök for guidance, input, support and a lot of interesting discussions. I also want to thank my co-supervisor Ann-Sophie Cans for introducing me to the lovely world of chromaffin vesicles, input, support and very nice discussions, improving the structure of this thesis and the illustration fig.3c.

Thanks to all of my collaborators in the different papers, Vladimir Zhdanov for equations, insight and nice discussions. Hoda Fathali being open to share rather creative experimental proceedings, enriching my life with the experience of acquiring biological samples and a lot of fun. Thanks to Laura de Battice, for being a really good friend, hopefully we can still turn those DNA-vesicle experiments into a paper.

Thanks to Peter Jönsson and Lisa Simonsson for introducing me to the world of Biological physics. Thanks to Jennie Sjöhamn for introducing me to the joys of cell culturing and protein purification.

Also, I would like to thank my former and present roommates over the years, Björn Johansson Fast, Nagma Parveen, Nadia Peerbom, Karin Norling and Mattias Sjöberg, thank you for good times and interesting discussions (perhaps not always scientific).

Last but not least, I would like to thank my wife and children for sharing life and being there for me, even at times when I have not felt so well.

Thanks to all former and present colleagues at the Biological Physics group.

A big thank you to GMV for financing.

8 Publication

Hydrodynamic separation of proteins in supported lipid bilayers confined by gold barriers
Björn Johansson, Thomas Olsson, Peter Jönsson and Fredrik Höök
Soft Matter 9, 9414-9419 (2013).

Total internal reflection fluorescence microscopy for determination of size of individual immobilized vesicles: Theory and experiment
T. Olsson, V. P. Zhdanov, and F. Höök,
J. Appl. Phys., vol. 118, no. 6, p. 064702, Aug. 2015.

9 Bibliography

1. Overington, J. P., Al-Lazikani, B. & Hopkins, A. L. How many drug targets are there? *Nat. Rev. Drug Discov.* **5,** 993–996 (2006).
2. Bangham, A. D., De Gier, J. & Greville, G. D. Osmotic properties and water permeability of phospholipid liquid crystals. *Chem. Phys. Lipids* **1,** 225–246 (1967).
3. Edwards, K. A. & Baeumner, A. J. Liposomes in analyses. *Talanta* **68,** 1421–31 (2006).
4. Edwards, K. A. *Liposomes in Analytical Methodologies*. (2016). doi:10.4032/9789814669276
5. Christensen, S. M. & Stamou, D. G. Sensing-applications of surface-based single vesicle arrays. *Sensors (Basel).* **10,** 11352–68 (2010).
6. Kunding, A. H., Mortensen, M. W., Christensen, S. M. & Stamou, D. A fluorescence-based technique to construct size distributions from single-object measurements: application to the extrusion of lipid vesicles. *Biophys. J.* **95,** 1176–88 (2008).
7. Lohr, C., Kunding, A. H., Bhatia, V. K. & Stamou, D. Constructing size distributions of liposomes from single-object fluorescence measurements. *Methods Enzymol.* **465,** 143–60 (2009).
8. Winkler, H. Commentary the Composition of Adrenal Chromaffin Granules : an Assessment of controversial results. (1976).
9. Fathali, H. & Cans, A. S. Amperometry methods for monitoring vesicular quantal size and regulation of exocytosis release. *Pflugers Arch. Eur. J. Physiol.* **470,** 125–134 (2018).
10. Fathali, H., Dunevall, J., Majdi, S. & Cans, A.-S. Extracellular Osmotic Stress Reduces the Vesicle Size while Keeping a Constant Neurotransmitter Concentration. doi:10.1021/acschemneuro.6b00350
11. Hooke, R. *Micrographia by Robert Hooke, 1665*. (The British Library, 1665).
12. The Cells in Your Body - Science NetLinks. Available at: http://sciencenetlinks.com/student-teacher-sheets/cells-your-body/. (Accessed: 4th May 2018)
13. Bianconi, E. *et al.* An estimation of the number of cells in the human body. *Ann. Hum. Biol.* **40,** 463–471 (2013).
14. Perez-Vilar, J., Mabolo, R., McVaugh, C. T., Bertozzi, C. R. & Boucher, R. C. Mucin granule intraluminal organization in living mucous/goblet cells: Roles of protein post-translational modifications and secretion. *J. Biol. Chem.* **281,** 4844–4855 (2006).
15. Deyrup-Olsen, I. & Luchtel, D. L. Secretion of Mucous Granules and Other Membrane-Bound Structures: A Look Beyond Exocytosis. *Int. Rev. Cytol.* **183,** 95–141 (1998).
16. Risselada, H. J. & Grubmüller, H. How SNARE molecules mediate membrane fusion: Recent insights from molecular simulations. *Curr. Opin. Struct. Biol.* **22,** 187–196 (2012).
17. Rudnick, G. Vesicular ATP transport is a hard (V)NUT to crack. *Proc. Natl. Acad. Sci. U. S. A.* **105,** 5949–50 (2008).
18. Battles, V. E. Nervous System Parts and Functions Medical Terminology :: Available at: https://prohealthinsight.com/body-systems/nervous-system/nervous-system-parts-and-functions-medical-terminology/. (Accessed: 25th July 2018)
19. Fathali, H. Development of new analytical techniques to probe and characterize secretory vesicles. (Chalmers Technical College, 2017).
20. Harrison, P., Gardiner, C. & Sargent, I. L. *Extracellular Vesicles in health and disease*. **1660,** (2017).
21. Schneider, A. & Simons, M. Exosomes: Vesicular carriers for intercellular communication in neurodegenerative disorders. *Cell Tissue Res.* **352,** 33–47 (2013).
22. Rutter, G. A. & Tsuboi, T. Kiss and run exocytosis of dense core secretory vesicles. *Neuroreport* **15,** 79–81 (2004).

23. Alberts, B. *et al. Molecular biology of the cell*. *Biochemistry and Molecular Biology Education* **36,** (Garland Science, 2007).
24. Singer, A. S. J. & Nicolson, G. L. The Fluid Mosaic Model of the Structure of Cell Membranes. *Science (80-.).* **175,** 720–731 (1972).
25. Janmey, P. A. & Kinnunen, P. K. J. Biophysical properties of lipids and dynamic membranes. *Trends Cell Biol.* **16,** 538–546 (2006).
26. Phillips, R., Kondev, J., Theriot, J., Garcia, H. & Chasan, B. *Physical Biology of the Cell*. *American Journal of Physics* **78,** (2010).
27. German, C. L., Baladi, M. G., McFadden, L. M., Hanson, G. R. & Fleckenstein, A. E. Regulation of the Dopamine and Vesicular Monoamine Transporters: Pharmacological Targets and Implications for Disease. *Pharmacol. Rev.* **67,** 1005–1024 (2015).
28. Brunner, J., Graham, D. E., Hauser, H. & Semenza, G. Ion and sugar permeabilities of lecithin bilayers: Comparison of curved and planar bilayers. *J. Membr. Biol.* **57,** 133–141 (1980).
29. Walter, A. & Gutknecht, J. Permeability of small nonelectrolytes through lipid bilayer membranes. *J. Membr. Biol.* **90,** 207–217 (1986).
30. Raven, J. A. *Energetics and transport in aquatic plants*. *4* (Alan R. Liss, Inc., 1984).
31. Brändén, M., Tabaei, S. R., Fischer, G., Neutze, R. & Höök, F. Refractive-index-based screening of membrane-protein-mediated transfer across biological membranes. *Biophys. J.* **99,** 124–33 (2010).
32. Mathai, J. C., Tristram-Nagle, S., Nagle, J. F. & Zeidel, M. L. Structural determinants of water permeability through the lipid membrane. *J. Gen. Physiol.* **131,** 69–76 (2008).
33. Shimanouchi, T., Ishii, H., Yoshimoto, N., Umakoshi, H. & Kuboi, R. Calcein permeation across phosphatidylcholine bilayer membrane: Effects of membrane fluidity, liposome size, and immobilization. *Colloids Surfaces B Biointerfaces* **73,** 156–160 (2009).
34. Xiang, T. X. & Anderson, B. D. Permeability of acetic acid across gel and liquid-crystalline lipid bilayers conforms to free-surface-area theory. *Biophys. J.* **72,** 223–237 (1997).
35. Jarrow.
36. Fettiplace, R. The influence of the lipid on the water permeability of artificial membranes. *Biochim. Biophys. Acta - Biomembr.* **513,** 1–10 (1978).
37. Kwant, W. O. & Seeman, P. The erythrocyte ghost is a perfect osmometer. *J. Gen. Physiol.* **55,** 208–219 (1970).
38. Morris, S. J., Schultens, H. A. & Schober, R. An osmometer model for changes in the buoyant density of chromaffin granules. *Biophys. J.* **20,** 33–48 (1977).
39. Gier, J. de. Liposomes Recognized as Osmometers. *J. Liposome Res.* **5,** 365–369 (1995).
40. Pencer, J., White, G. F. & Hallett, F. R. Osmotically induced shape changes of large unilamellar vesicles measured by dynamic light scattering. *Biophys. J.* **81,** 2716–2728 (2001).
41. Lerebours, B., Wehrli, E. & Hauser, H. Thermodynamic stability and osmotic sensitivity of small unilamellar phosphatidylcholine vesicles. *Biochim. Biophys. Acta - Biomembr.* **1152,** 49–60 (1993).
42. Edwards, K., Johnsson, M., Karlsson, G. & Silvander, M. Preparations of Small Unilamellar Liposomes. *Biophys. J.* **73,** 258–266 (1997).
43. Jin, A. J., Huster, D., Gawrisch, K. & Nossal, R. Light scattering characterization of extruded lipid vesicles. *Eur. Biophys. J. with Biophys. Lett.* **28,** 187–199 (1999).
44. Jönsson, P., Jonsson, M. P., Tegenfeldt, J. O. & Höök, F. A method improving the accuracy of fluorescence recovery after photobleaching analysis. *Biophys. J.* **95,** 5334–48 (2008).
45. Ertel, A., Marangoni, A. G., Marsh, J., Hallett, F. R. & Wood, J. M. Mechanical properties of vesicles. I. Coordinated analysis of osmotic swelling and lysis. *Biophys. J.* **64,** 426–

434 (1993).
46. Hallett, F. R., Marsh, J., Nickel, B. G. & Wood, J. M. Mechanical properties of vesicles. II. A model for osmotic swelling and lysis. *Biophys. J.* **64,** 435–42 (1993).
47. Hallett, F. R., Marsh, J., Nickel, B. G. & Wood, J. M. Mechanical properties of vesicles. II. A model for osmotic swelling and lysis. *Biophys. J.* **64,** 435–442 (1993).
48. Claessens, M. M. A. E., Leermakers, F. A. M., Hoekstra, F. A. & Stuart, M. A. C. Osmotic shrinkage and reswelling of giant vesicles composed of dioleoylphosphatidylglycerol and cholesterol. *Biochim. Biophys. Acta* **1778,** 890–5 (2008).
49. Jansen, M. & Blume, A. A comparative study of diffusive and osmotic water permeation across bilayers composed of phospholipids with different head groups and fatty acyl chains. *Biophys. J.* **68,** 997–1008 (1995).
50. Mathai, J. C. & Zeidel, M. L. Measurement of water and solute permeability by stopped-flow fluorimetry. *Methods Mol. Biol.* **400,** 323–32 (2007).
51. Chen, P. Y., Pearce, D. & Verkman, A. S. Membrane water and solute permeability determined quantitatively by self-quenching of an entrapped fluorophore. *Biochemistry* **27,** 5713–5718 (1988).
52. Peterlin, P., Jakli, G. & Pisanski, T. Determining membrane permeability of giant phospholipid vesicles from a series of videomicroscopy images. *Meas. Sci. Technol.* **20,** (2009).
53. Lande, M., Donovan, J. & Zeidel, M. L. The Relationship between Membrane Fluidity and Permeabilities to Water, Solutes, Ammonia, and Protons.
54. Mathai, J. C. *et al.* Functional analysis of aquaporin-1 deficient red cells: The colton-null phenotype. *J. Biol. Chem.* **271,** 1309–1313 (1996).
55. Pfeuffer, J. *et al.* Expression of aquaporins in Xenopus laevis oocytes and glial cells as detected by diffusion-weighted 1H NMR spectroscopy and photometric swelling assay. *Biochim. Biophys. Acta - Mol. Cell Res.* **1448,** 27–36 (1998).
56. Stillwell, W. *An Introduction to Biological Membranes*. *An Introduction to Biological Membranes* (Elsevier, 2013). doi:10.1016/B978-0-444-52153-8.00014-3
57. Agre, P. Aquaporin water channels (Nobel Lecture). *Angew. Chem. Int. Ed. Engl.* **43,** 4278–90 (2004).
58. Mosharov, E. V, Gong, L.-W., Khanna, B., Sulzer, D. & Lindau, M. Intracellular patch electrochemistry: regulation of cytosolic catecholamines in chromaffin cells. *J. Neurosci.* **23,** 5835–5845 (2003).
59. 16:0-18:1 PC | Avanti Polar Lipids. Available at: https://avantilipids.com/product/850457/. (Accessed: 6th May 2018)
60. Israelachvili, J. N., Mitchell, D. J. & Ninham, B. W. Theory of self-assembly of hydrocarbon amphiphiles into micelles and bilayers. *J. Chem. Soc. Faraday Trans. 2* **72,** 1525 (1976).
61. Israelachvili, J. N. *Intermolecular and Surface Forces*. *Intermolecular and Surface Forces* (Elsevier, 2011). doi:10.1016/B978-0-12-375182-9.10020-X
62. van Hoogevest, P., de Gier, J. & de Kruijff, B. Determination of the size of the packing defects in dimyristoylphosphatidylcholine bilayers, present at the phase transition temperature. *FEBS Lett.* **171,** 160–164 (1984).
63. Haest, C. W. M., De Gier, J., Van Es, G. A., Verkleij, A. J. & Van Deenen, L. L. M. Fragility of the permeability barrier of Escherichia coli. *BBA - Biomembr.* **288,** 43–53 (1972).
64. Blank, M. & Markov, M. *Electromagnetic Fields and Biomembranes*. (Plenum Press, 1988). doi:10.1007/978-1-4615-9507-6
65. Seu, K. J., Cambrea, L. R., Everly, R. M. & Hovis, J. S. Influence of lipid chemistry on membrane fluidity: Tail and headgroup interactions. *Biophys. J.* **91,** 3727–3735 (2006).
66. Maherani, B., Arab-Tehrany, E., Kheirolomoom, A., Geny, D. & Linder, M. Calcein release behavior from liposomal bilayer; Influence of

physicochemical/mechanical/structural properties of lipids. *Biochimie* **95,** 2018–2033 (2013).
67. Amatore, C. *et al.* Correlation between vesicle quantal size and fusion pore release in chromaffin cell exocytosis. *Biophys. J.* **88,** 4411–4420 (2005).
68. Bo, L. & Waugh, R. E. Determination of bilayer membrane bending stiffness by tether formation from giant, thin-walled vesicles. *Biophys. J.* **55,** 509–517 (1989).
69. Callan-Jones, A., Sorre, B. & Bassereau, P. Curvature-driven lipid sorting in biomembranes. *Cold Spring Harbor Perspectives in Biology* **3,** 1–14 (2011).
70. Sorre, B. *et al.* Curvature-driven lipid sorting needs proximity to a demixing point and is aided by proteins. *Proc. Natl. Acad. Sci. U. S. A.* **106,** 5622–5626 (2009).
71. Kaksonen, M. & Roux, A. Mechanisms of clathrin-mediated endocytosis. *Nat. Rev. Mol. Cell Biol.* **19,** 313–326 (2018).
72. Phase Transition Temperatures for Glycerophospholipids | Avanti Polar Lipids. Available at: https://avantilipids.com/tech-support/physical-properties/phase-transition-temps/. (Accessed: 5th May 2018)
73. Jönsson, P., Beech, J. P., Tegenfeldt, J. O. & Höök, F. Shear-Driven Motion of Supported Lipid Bilayers in Microfluidic Channels. *J. Am. Chem. Soc.* **131,** 5294–5297 (2009).
74. Mouritsen, O. G. & Bloom, M. Mattress model of lipid-protein interactions in membranes. *Biophys. J.* **46,** 141–153 (1984).
75. Szoka, F. & Papahadjopoulos, D. COMPARATIVE PROPERTIES AND METHODS OF PREPARATION OF LIPID VESICLES (LIPOSOMES). *Annu. Rev. Biophys. Bioeng.* **9,** 467–508 (1980).
76. Olson, F., Hunt, C. A., Szoka, F. C., Vail, W. J. & Papahadjopoulos, D. Preparation of liposomes of defined size distribution by extrusion through polycarbonate membranes. *Biochim. Biophys. Acta - Biomembr.* **557,** 9–23 (1979).
77. Hope, M. J., Bally, M. B., Webb, G. & Cullis, P. R. Production of large unilamellar vesicles by a rapid extrusion procedure. Characterization of size distribution, trapped volume and ability to maintain a membrane potential. *Biochimica et Biophysica Acta (BBA) - Biomembranes* **812,** 55–65 (1985).
78. Traikia, M., Warschawski, D. E., Recouvreur, M., Cartaud, J. & Devaux, P. F. Formation of unilamellar vesicles by repetitive freeze-thaw cycles: characterization by electron microscopy and P-31-nuclear magnetic resonance. *Eur. Biophys. J.* **29,** 184–195 (2000).
79. Hope, M. J., Bally, M. B., Mayer, L. D., Janoff, A. S. & Cullis, P. R. Generation of multilamellar and unilamellar phospholipid vesicles. *Chem. Phys. Lipids* **40,** 89–107 (1986).
80. Wink, T., Van Zuilen, S. J., Bult, A. & Van Bennekom, W. P. Liposome-Mediated Enhancement of the Sensitivity in Immunoassays of Proteins and Peptides in Surface Plasmon Resonance Spectrometry. *Anal. Chem.* **70,** 827–832 (1998).
81. Ohlsson, G. *et al.* Solute transport on the sub 100 ms scale across the lipid bilayer membrane of individual proteoliposomes. *Lab on a Chip* **12,** 4635 (2012).
82. Tonnesen, A., Christensen, S. M., Tkach, V. & Stamou, D. Geometrical membrane curvature as an allosteric regulator of membrane protein structure and function. *Biophys. J.* **106,** 201–9 (2014).
83. Reeves, J. P. & Dowben, R. M. Formation and properties of thin-walled phospholipid vesicles. *J. Cell. Physiol.* **73,** 49–60 (1969).
84. De Gier, J., Mandersloot, J. G. & Van Deenen, L. L. M. Lipid composition and permeability of liposomes. *Biochim. Biophys. Acta - Biomembr.* **150,** 666–675 (1968).
85. Paula, S., Volkov, A. G., Van Hoek, A. N., Haines, T. H. & Deamer, D. W. Permeation of protons, potassium ions, and small polar molecules through phospholipid bilayers as a function of membrane thickness. *Biophys. J.* **70,** 339–48 (1996).
86. Cohen, B. E. The permeability of liposomes to nonelectrolytes. I. Activation energies

for permeation. *J. Membr. Biol.* **20,** 205–234 (1975).
87. Sacerdote, M. G. & Szostak, J. W. Semipermeable lipid bilayers exhibit diastereoselectivity favoring ribose. *Proc. Natl. Acad. Sci. U. S. A.* **102,** 6004–8 (2005).
88. Ohlsson, G. *et al.* Solute transport on the sub 100 ms scale across the lipid bilayer membrane of individual proteoliposomes. *Lab Chip* **12,** 4635–43 (2012).
89. Lande, M. B., Donovan, J. M. & Zeidel, M. L. The relationship between membrane fluidity and permeabilities to water, solutes, ammonia, and protons. *J. Gen. Physiol.* **106,** 67–84 (1995).
90. Lu, T., Wang, Z., Ma, Y., Zhang, Y. & Chen, T. Influence of polymer size, liposomal composition, surface charge, and temperature on the permeability of pH-sensitive liposomes containing lipid-anchored poly(2-ethylacrylic acid). *Int. J. Nanomedicine* **7,** 4917–4926 (2012).
91. Stillwell, W. Membranes and Human Health. *An Introd. to Biol. Membr.* 339–355 (2013). doi:10.1016/B978-0-444-52153-8.00015-5
92. Laouini, A. *et al.* Preparation, Characterization and Applications of Liposomes: State of the Art. *J. Colloid Sci. Biotechnol.* **1,** 147–168 (2012).
93. Johansson, B., Olsson, T., Jönsson, P. & Höök, F. Hydrodynamic separation of proteins in supported lipid bilayers confined by gold barriers. *Soft Matter* **9,** 9414 (2013).
94. Block, S., Fast, B. J., Lundgren, A., Zhdanov, V. P. & Höök, F. Two-dimensional flow nanometry of biological nanoparticles for accurate determination of their size and emission intensity. *Nat. Commun.* **7,** 12956 (2016).
95. Voskuhl, J. & Ravoo, B. J. Molecular recognition of bilayer vesicles. *Chem. Soc. Rev.* **38,** 495–505 (2009).
96. Sapala, A. R., Dhawan, S. & Haridas, V. Vesicles: self-assembly beyond biological lipids. *RSC Adv.* **7,** 26608–26624 (2017).
97. Cho, N. J., Hwang, L. Y., Solandt, J. J. R. & Frank, C. W. Comparison of extruded and sonicated vesicles for planar bilayer self-assembly. *Materials (Basel).* **6,** 3294–3308 (2013).
98. Gier, J. De. Osmotic behaviour and permeability properties of liposomes. **c,** 187–196 (1993).
99. Lu, N.-Y., Yang, K., Li, J.-L., Yuan, B. & Ma, Y.-Q. Vesicle deposition and subsequent membrane–melittin interactions on different substrates: A QCM-D experiment. *Biochim. Biophys. Acta - Biomembr.* **1828,** 1918–1925 (2013).
100. Park Systems. Bio Atomic Force Microscope: Liposomes and Vesicles. Available at: https://www.parksystems.com/index.php/applications/life-science/micro-and-molecular-biology/132-liposomes-and-vesicles. (Accessed: 7th June 2018)
101. Edwards, K. A. *Liposomes in Analytical Methodologies*. (Pan Stanford, 2016). doi:10.1201/b19912
102. Cooper, M. A., Hansson, A., Löfås, S. & Williams, D. H. A vesicle capture sensor chip for kinetic analysis of interactions with membrane-bound receptors. *Anal. Biochem.* **277,** 196–205 (2000).
103. Bally, M., Graule, M., Parra, F., Larson, G. & Höök, F. A virus biosensor with single virus-particle sensitivity based on fluorescent vesicle labels and equilibrium fluctuation analysis. *Biointerphases* **8,** 1–9 (2013).
104. Gunnarsson, A. *et al.* Kinetics of ligand binding to membrane receptors from equilibrium fluctuation analysis of single binding events. *J. Am. Chem. Soc.* **133,** 14852–14855 (2011).
105. Fenzl, C., Hirsch, T. & Baeumner, A. J. Liposomes with High Refractive Index Encapsulants as Tunable Signal Amplification Tools in Surface Plasmon Resonance Spectroscopy. *Anal. Chem.* **87,** 11157–11163 (2015).
106. Wahlsten, O. *et al.* Equilibrium-Fluctuation Analysis for Interaction Studies between Natural Ligands and Single G Protein-Coupled Receptors in Native Lipid Vesicles.

Langmuir **31,** 10774–10780 (2015).
107. Rupert, D. L. M., Shelke, G. V., Emilsson, G. & Claudio, V. The Concentration of a Sub-Population of Extracellular Vesicles Identified using Dual-Wavelength Surface Plasmon Resonance. 1–12
108. Rupert, D. L. M. *et al.* Dual-Wavelength Surface Plasmon Resonance for Determining the Size and Concentration of Sub-Populations of Extracellular Vesicles. *Anal. Chem.* **88,** 9980–9988 (2016).
109. Im, H., Yang, K., Lee, H. & Castro, C. M. in 133–141 (2017). doi:10.1007/978-1-4939-7253-1_11
110. Brändén, M., Dahlin, S. & Höök, F. Label-free measurements of molecular transport across liposome membranes using evanescent-wave sensing. *ChemPhysChem* **9,** 2480–2485 (2008).
111. Ohlsson, G. *et al.* Solute transport on the sub 100 ms scale across the lipid bilayer membrane of individual proteoliposomes. *Lab Chip* **12,** 4635–43 (2012).
112. Tabaei, S. R., Rabe, M., Zetterberg, H., Zhdanov, V. P. & Höök, F. Single lipid vesicle assay for characterizing single-enzyme kinetics of phospholipid hydrolysis in a complex biological fluid. *J. Am. Chem. Soc.* **135,** 14151–14158 (2013).
113. Stengel, G., Simonsson, L., Campbell, R. A. & Höök, F. Determinants for membrane fusion induced by cholesterol-modified DNA zippers. *J. Phys. Chem. B* **112,** 8264–8274 (2008).
114. Christensen, S. M. & Stamou, D. Surface-based lipid vesicle reactor systems: fabrication and applications. *Soft Matter* **3,** 828 (2007).
115. González, M., Argaraña, C. E. & Fidelio, G. D. Extremely high thermal stability of streptavidin and avidin upon biotin binding. *Biomol. Eng.* **16,** 67–72 (1999).
116. A complete microscope history - Who invented the microscope? Available at: http://www.history-of-the-microscope.org/history-of-the-microscope-who-invented-the-microscope.php. (Accessed: 7th May 2018)
117. The Diffraction Barrier in Optical Microscopy | MicroscopyU. Available at: https://www.microscopyu.com/techniques/super-resolution/the-diffraction-barrier-in-optical-microscopy. (Accessed: 21st April 2018)
118. ATTO-TEC GmbH - ATTO 647N. Available at: https://www.atto-tec.com/attotecshop/product_info.php?info=p114_atto-647n.html&XTCsid=1b064d33da8a892acf3698f1d99566fd. (Accessed: 12th April 2018)
119. The Molecular Probes Handbook.
120. Axelrod, D. Cell-substrate contacts illuminated by total internal reflection fluorescence. *J. Cell Biol.* **89,** 141–145 (1981).
121. Axelrod, D., Koppel, D. E., Schlessinger, J., Elson, E. & Webb, W. W. Mobility measurement by analysis of fluorescence photobleaching recovery kinetics. *Biophys. J.* **16,** 1055–1069 (1976).
122. Johansson, B., Olsson, T., Jönsson, P. & Höök, F. Hydrodynamic separation of proteins in supported lipid bilayers confined by gold barriers. doi:10.1039/c3sm51673c
123. Peter Jönsson. frap_analysis - File Exchange - MATLAB Central. Available at: https://se.mathworks.com/matlabcentral/fileexchange/29388-frap-analysis. (Accessed: 21st April 2018)
124. Hamann, S. *et al.* Measurement of Cell Volume Changes by Fluorescence Self-Quenching. in *Journal of Fluorescence* **12,** 139–145 (2002).
125. Belinda, C. British Museum — The Lycurgus Cup. Available at: https://britishmuseum.tumblr.com/post/120689869617/the-lycurgus-cup. (Accessed: 29th March 2018)
126. Heroes, Heroines, and History: August 2017. Available at: http://www.hhhistory.com/2017/08/. (Accessed: 8th May 2018)

127. Wood, R. W. XLII. *On a remarkable case of uneven distribution of light in a diffraction grating spectrum*. *Philos. Mag. Ser. 6* **4,** 396–402 (1902).
128. Maystre, D. & Daniel. in *Plasmonics, Springer Series in Optical Sciences, Volume 167. ISBN 978-3-642-28078-8. Springer-Verlag Berlin Heidelberg, 2012, p. 39* 39–83 (2012). doi:10.1007/978-3-642-28079-5_2
129. Rayleigh, L. On the Dynamical Theory of Gratings. *Proc. R. Soc. A Math. Phys. Eng. Sci.* **79,** 399–416 (1907).
130. Fano, U. The Theory of Anomalous Diffraction Gratings and of Quasi-Stationary Waves on Metallic Surfaces (Sommerfeld's Waves). *J. Opt. Soc. Am.* **31,** 213 (1941).
131. Kretschmann, E. & Raether, H. Radiative Decay of Non Radiative Surface Plasmons Excited by Light. *Zeitschrift fur Naturforschung - Section A Journal of Physical Sciences* **23,** 2135–2136 (1968).
132. Otto, A. Excitation of nonradiative surface plasma waves in silver by the method of frustrated total reflection. *Zeitschrift für Phys. A Hadron. Nucl.* **216,** 398–410 (1968).
133. Liedberg, B., Nylander, C. & Lunström, I. Surface plasmon resonance for gas detection and biosensing. *Sensors and Actuators* **4,** 299–304 (1983).
134. Healthcare, G. *BIAcore concentration analysis*. (2008).
135. Handley, J. Product Review: Quartz Crystal Microbalances. *Anal. Chem.* **73,** 225 A-229 A (2001).
136. Liedberg, B., Nylander, C. & Lunström, I. Surface plasmon resonance for gas detection and biosensing. *Sensors and Actuators* **4,** 299–304 (1983).
137. Mikhail Polyanskiy. Optical constants of Au (Gold). Available at: https://refractiveindex.info/?shelf=main&book=Au&page=Johnson. (Accessed: 29th March 2018)
138. Johnson, P. B. & Christy, R. W. Optical constants of the noble metals. *Phys. Rev. B* **6,** 4370–4379 (1972).
139. Liedberg, B., Lundström, I. & Stenberg, E. Principles of biosensing with an extended coupling matrix and surface plasmon resonance. *Sensors Actuators B. Chem.* **11,** 63–72 (1993).
140. Liedberg, B., Nylander, C. & Lundstrom, I. Biosensing with Surfacing Plasmon Resonance - How It All Started. *Biosens. Bioelectron.* **10,** i–ix (1995).
141. Jung, L. S. *et al.* Quantitative Interpretation of the Response of Surface Plasmon Resonance Sensors to Adsorbed Films. *Langmuir* **14,** 5636–5648 (1998).
142. De Feijter, J. A., Benjamins, J. & Veer, F. A. Ellipsometry as a tool to study the adsorption behavior of synthetic and biopolymers at the air-water interface. *Biopolymers* **17,** 1759–1772 (1978).
143. Shoup, D. & Szabo, A. Chronoamperometric current at finite disk electrodes. *J. Electroanal. Chem. Interfacial Electrochem.* **140,** 237–245 (1982).
144. Austin-Harrison, D. S. & Johnson, D. C. Pulsed amperometric detection based on direct and indirect anodic reactions: A review. *Electroanalysis* **1,** 189–197 (1989).
145. Talmon, Y., Burns, J. L., Chestnut, M. H. & Siegel, D. P. Timeresolved cryotransmission electron microscopy. *J. Electron Microsc. Tech.* **14,** 6–12 (1990).
146. Hallett, F. R., Nickel, B., Samuels, C. & Krygsman, P. H. Determination of vesicle size distributions by freezefracture electron microscopy. *J. Electron Microsc. Tech.* **17,** 459–466 (1991).
147. Filipe, V., Hawe, A. & Jiskoot, W. Critical evaluation of nanoparticle tracking analysis (NTA) by NanoSight for the measurement of nanoparticles and protein aggregates. *Pharm. Res.* **27,** 796–810 (2010).
148. Panas, A. *et al.* Nanoscale Material Characterization : a Review of the use of Nanoparticle Tracking Analysis (NTA). *Beilstein J. Nanotechnol.* **5,** 1590–1602 (2014).
149. Frisken, B. J. Revisiting the method of cumulants for the analysis of dynamic light-

scattering data. *Appl. Opt.* **40,** 4087 (2001).
150. Olsson, T., Zhdanov, V. P. & Höök, F. Total internal reflection fluorescence microscopy for determination of size of individual immobilized vesicles: Theory and experiment. *J. Appl. Phys.* **118,** 064702 (2015).
151. Mui, B., Chow, L. & Hope, M. J. Extrusion Technique to Generate Liposomes of Defined Size. *Methods Enzymol.* **367,** 3–14 (2003).
152. Fathali, H., Dunevall, J., Majdi, S. & Cans, A.-S. Extracellular osmotic stress reduces the vesicle size while keeping a constant neurotransmitter concentration. *ACS Chem. Neurosci.* (2016).
153. Li, X., Majdi, S., Dunevall, J., Fathali, H. & Ewing, A. G. Quantitative measurement of transmitters in individual vesicles in the cytoplasm of single cells with nanotip electrodes. *Angew. Chemie Int. Ed.* **54,** 11978–11982 (2015).
154. Albillos, A. *et al.* The exocytotic event in chromaffin cells revealed by patch amperometry. *Nature* **389,** 509–512 (1997).
155. Morris, S. J., Schultens, H. A. & Schober, R. An osmometer model for changes in the buoyant density of chromaffin granules. *Biophys. J.* **20,** 33–48 (1977).
156. Weiner, N. & Jardetzky, O. A Study of Catecholamine Nucleotide Complexes by Nuclear Magnetic Resonance Spectroscopy. *Naunyn-Schmiedebergs Arch. exp. Path. u. Pharmak.* **248,** 308–318 (1964).
157. Winkler, H. & Westhead, E. The Molecular of Adrenal Chromaffin Granules. *Neuroscience* **5,** 1803–1823 (1980).
158. Hale, G. M. & Querry, M. R. Optical Constants of Water in the 200-nm to 200-μm Wavelength Region. *Appl. Opt.* **12,** 555 (1973).
159. Kedenburg, S., Vieweg, M., Gissibl, T. & Giessen, H. Linear refractive index and absorption measurements of nonlinear optical liquids in the visible and near-infrared spectral region. *Opt. Mater. Express* **2,** 1588 (2012).
160. Russell, J. T. The Secretory Vesicle in Processing and Secretion of Neuropeptides. *Curr. Top. Membr. Transp.* **31,** 277–312 (1987).
161. Search, H., Journals, C., Contact, A., Iopscience, M. & Address, I. P. The spatial variation of the refractive index in biological cells. **369,** (1996).
162. Royal society of chemistry. Cholesterol. Available at: http://www.chemspider.com/Chemical-Structure.5775.html. (Accessed: 4th June 2018)
163. Zhao, H., Brown, P. H. & Schuck, P. On the distribution of protein refractive index increments. *Biophys. J.* **100,** 2309–17 (2011).
164. Winkler, H. The composition of adrenal chromaffin granules: An assessment of cotroversial results. *Neuroscience* **1,** 65–80 (1976).
165. Royal society of chemistry. Leu-enkephalin. Available at: http://www.chemspider.com/Chemical-Structure.406229.html. (Accessed: 3rd July 2018)
166. Royal society of chemistry. Met-enkephalin. Available at: http://www.chemspider.com/Chemical-Structure.391597.html?rid=08b658b0-8bb4-4035-ad95-bfdb0dffb8c7&page_num=0. (Accessed: 3rd July 2018)
167. Royal society of chemistry. Adenosine triphosphate. Available at: http://www.chemspider.com/Chemical-Structure.5742.html. (Accessed: 3rd July 2018)
168. Royal society of chemistry. Epinephrine. Available at: http://www.chemspider.com/Chemical-Structure.5611.html?rid=5aa80ccc-74c3-4e47-9002-079a68b83342. (Accessed: 4th June 2018)
169. Fischer, H., Polikarpov, I. & Craievich, A. F. Average protein density is a molecular-weight-dependent function. *Protein Sci.* **13,** 2825–2828 (2009).
170. Antonenko, Y. N., Pohl, P. & Denisov, G. A. Permeation of ammonia across bilayer lipid

membranes studied by ammonium ion selective microelectrodes. *Biophys. J.* **72,** 2187–95 (1997).